Progress In Electromagnetics Research, PIER 37, 143–190, 2002

A COMPOSITE MODEL FOR ESTIMATION OF POLARIMETRIC THERMAL EMISSION FROM FOAM-COVERED WIND-DRIVEN OCEAN SURFACE

Y. Zhang, Y. E. Yang, and J. A. Kong

Research Laboratory of Electronics
Department of Electronic Engineering and Computer Science
Massachusetts Institute of Technology
Cambridge, MA 02139, USA

Abstract—This paper presents theoretical studies of polarimetric thermal emission from foam-covered ocean surface based on a composite volume and rough surface scattering model using the radiative transfer theory. The sea foam is modeled as a layer containing randomly distributed thin-film water bubbles. The small perturbation method (SPM) is used for random rough ocean surface, where the bistatic scattering is calculated up to the second order. The radiative transfer equations with a rough interface are solved using an iterative technique. Model predictions are compared with empirical expressions for foam emissivity and with the WINDRAD measurement data.

1. INTRODUCTION

In the microwave remote sensing of ocean surface, the use of polarimetric passive techniques has shown potential for enhancing the retrieval of wind speed and directions [1]. Recent theoretical and experimental research activities have concentrated on studies of polarimetric thermal emissions regarding the anisotropic ocean surface assuming a smoothly varying surface profile [1–4]. However, under high wind conditions, the presence of breaking water waves, foam patches and bubbles will affect the polarimetric brightness temperatures of the plain ocean surface. The significance of foam on the ocean surface was recognized a long time ago [5], and several subsequent experiments performed have verified its importance [6, 7]. Previous studies of the foam contribution to the emissivity of ocean surface were based on empirical formulations [8, 9] derived from experimental data. Although several attempts at theoretically modeling the foam have been presented [10, 11], it is difficult to incorporate them with rough ocean surface. The more realistic modeling for foam-covered ocean surface has been proposed by Huang et al. [12], who consider the sea foam to be a layer with water particles over a rough sea surface.

However, it is not suited to model the sea foam as the layer of spherical water particles, since the sea foam is dominated by water bubbles [13]. In this chapter, we present the theoretical study on the polarimetric thermal emissions from foam-covered ocean surface based on a composite volume and rough surface scattering model using the radiative transfer theory. We model the locally foam-covered ocean surface as a random layer with water bubbles. The small perturbation method (SPM) is used for random rough ocean surface, where the bistatic scattering is calculated up to the second order. The radiative transfer equations for foam layer are solved using an iterative technique. The model predictions are compared with measurement data [14].

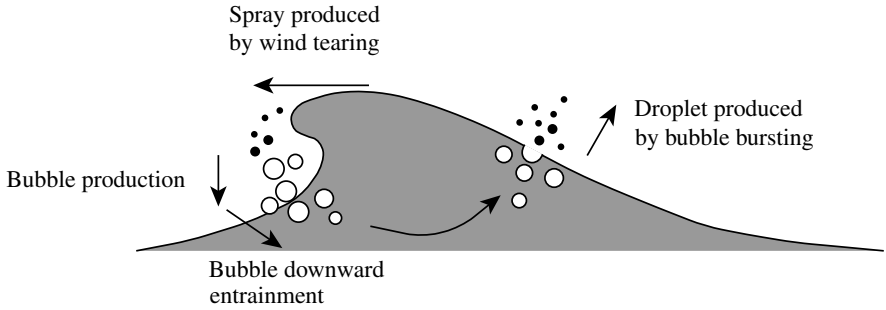

Figure 1. Generation of sea-foam.

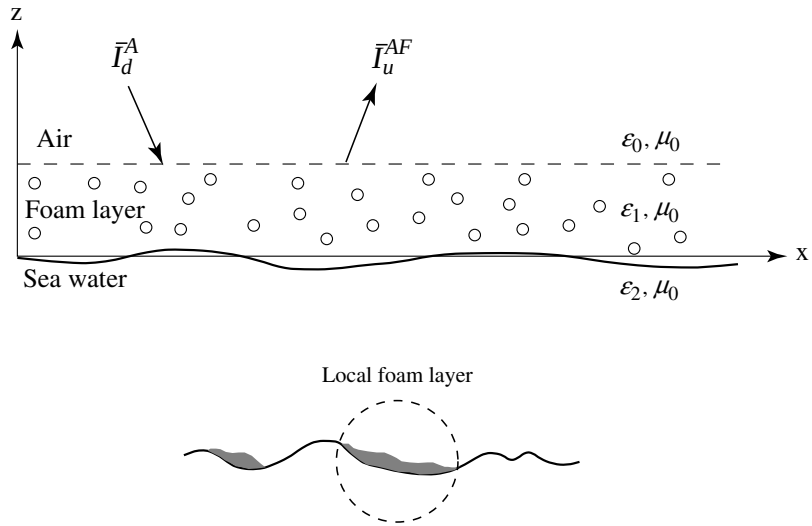

Figure 2. Configuration of local foam layer on wind-driven rough ocean surface.

2. FORMULATIONS FOR FOAM EMISSION

2.1. RT Equations for Foam Layer

Sea-foam is made of spray, small water droplets and air bubbles which are generated by wind tearing and further processions such as bubble production, bubble downward entrainment, and droplet produced by bubble bursting as illustrated in Fig. 1 [13]. Since the thermal emission from sea-foam is dominated by water bubbles, we simplify the sea-foam as a water bubble layer as shown in Fig. 2. For simplicity, the top

surface of the foam layer is considered to be a flat surface. Above the foam layer (region 1) is a half free space that is labeled as region 0 with ϵ_o, μ_o. The foam layer is specified by a foam thickness d_1, the inner bubble radius R, bubble film thinkness δ and permittivity ϵ_1, the fractional volume f_v of bubbles, the extinction coefficient κ_e, and the temperature profile $T(z)$. The background of the foam layer is considered to be free space with ϵ_o, μ_o. The sea water (region 2) is in the lower half space with permittivity ϵ_2, salinity S, and physical temperature T_o. The foam coverage is denoted by F, thus the coverage of the plain ocean surface is $1 - F$.

In the foam layer, the radiative transfer equation [15, page 229] is given by

$$\begin{aligned} \cos\theta \frac{d}{dz}\overline{I}(\theta,\phi,z) &= -\bar{\bar{\kappa}}_e(\theta,\phi)\cdot\overline{I}(\theta,\phi,z) \\ &\quad + \int_{4\pi} d\Omega' \,\overline{\overline{P}}(\theta,\phi,\theta',\phi')\cdot\overline{I}(\theta',\phi',z) + \overline{I}_T(\theta,\phi,z), \end{aligned} \tag{1}$$

where $\overline{\overline{P}}(\theta,\phi,\theta',\phi')$ is the phase matrix which is derived by using Mie theory in Appendix A. The phase matrix provides the contributions to the specific intensity $\overline{I}(\theta,\phi,z)$ in the direction (θ,ϕ) from the direction (θ',ϕ'). $\overline{\overline{\kappa}}_e$ is the extinction tensor. In this thesis, the specific intensity with the unit of W/m^2 is defined as

$$\overline{I}(\theta,\phi,z) = \frac{1}{\eta}\begin{bmatrix} \langle |E_v|^2 \rangle \\ \langle |E_h|^2 \rangle \\ 2\mathrm{Re}\langle E_v E_h^* \rangle \\ 2\mathrm{Im}\langle E_v E_h^* \rangle \end{bmatrix}, \tag{2}$$

where $\eta = \sqrt{\mu_o/\epsilon_o}$ is the free space impedance. $\overline{I}_T(\theta,\phi,z)$ is the intensity of the physical temperature and it is written as $\overline{I}_T(\theta,\phi,z) = \bar{\kappa}_a(\theta,\phi)CT(z)$. In this expression, $\bar{\kappa}_a$ is the absorption coefficient vector, $C = K_B/\lambda^2$ where K_B is the Boltzmann constant ($K_B = 1.380658 \times 10^{-23}$ J/K) and λ is the electromagnetic wavelength. We assume that the scatterers are bubbles and the absorption is isotropic, thus

$$\bar{\kappa}_a = \kappa_a \begin{bmatrix} 1 & 1 & 0 & 0 \end{bmatrix}^T. \tag{3}$$

As mentioned in the previous section, the foam layer is modeled as the composition of spherical water bubbles randomly distributed in the foam layer, therefore the extinction coefficient $\overline{\overline{\kappa}}_e(\theta,\phi)$ is a scalar, i.e., $\overline{\overline{\kappa}}_e(\theta,\phi) = \kappa_e$. The formulations of calculating κ_e and κ_a are provided in Appendix A. We assume that the temperature $T(z)$ in the foam layer is independent of elevation and it is equal to the temperature of the sea water, i.e., $T(z) = T_o$. Thus

$$\overline{I}_T(\theta,\phi,z) = \bar{\kappa}_a(\theta,\phi)CT_o. \tag{4}$$

Define the new specific intensities for $0 \le \theta < \pi/2$ as

$$\overline{I}_u(\theta,\phi,z) = \overline{I}(\theta,\phi,z), \tag{5}$$
$$\overline{I}_d(\theta,\phi,z) = \overline{I}(\pi-\theta,\phi,z), \tag{6}$$
$$\overline{I}_{Tu}(\theta,\phi,z) = \overline{I}_T(\theta,\phi,z), \tag{7}$$
$$\overline{I}_{Td}(\theta,\phi,z) = \overline{I}_T(\pi-\theta,\phi,z), \tag{8}$$

the RT equation (1) is split into two:

$$\begin{aligned}\cos\theta\frac{d}{dz}\overline{I}_u(\theta,\phi,z) &= -\kappa_e\overline{I}_u(\theta,\phi,z)\\ &\quad+\int_{\text{upper }2\pi} d\Omega'\,\overline{\overline{P}}(\theta,\phi,\theta',\phi')\cdot\overline{I}_u(\theta',\phi',z)\\ &\quad+\int_{\text{lower }2\pi} d\Omega'\,\overline{\overline{P}}(\theta,\phi,\pi-\theta',\phi')\cdot\overline{I}_d(\theta',\phi',z)\\ &\quad+\overline{I}_{Tu}(\theta,\phi),\end{aligned} \tag{9}$$

$$\begin{aligned}-\cos\theta\frac{d}{dz}\overline{I}_d(\theta,\phi,z) &= -\kappa_e\overline{I}_d(\theta,\phi,z)\\ &\quad+\int_{\text{upper }2\pi} d\Omega'\,\overline{\overline{P}}(\pi-\theta,\phi,\theta',\phi')\cdot\overline{I}_u(\theta',\phi',z)\\ &\quad+\int_{\text{lower }2\pi} d\Omega'\,\overline{\overline{P}}(\pi-\theta,\phi,\pi-\theta',\phi')\cdot\overline{I}_d(\theta',\phi',z)\\ &\quad+\overline{I}_{Td}(\theta,\phi).\end{aligned} \tag{10}$$

We assume that the thickness of the foam layer is much larger than the penetration depth of the electromagnetic wave. Under this assumption, there is no returned wave from the bottom of the foam layer. Thus the boundary conditions are:

on the upper boundary ($z = d_1$)

$$\overline{I}_d(\theta, \phi, d_1) = \overline{I}_d^A(\theta, \phi, d_1), \tag{11}$$

on the lower boundary ($z = 0$)

$$\overline{I}_u(\theta, \phi, 0) = 0, \tag{12}$$

where $\overline{I}_d^A(\theta, \phi, d_1)$ is the specific intensity of the atmospheric layer.

2.2. Solution of the RT Equation

To solve the RT equations (9) and (10), the iterative and numerical methods can be used. The iterative method is applied to scattering problems with small absorption which is the case for the foam layer, while the numerical method can be applied for strong absorption problems.

In the iterative method of solving the RT equations, we consider the integral terms as known from the lower order solutions, thus the RT equations for each step are in the form of an ordinary differential equation (ODE). The general form of the first order ODE is written as

$$\frac{dy(z)}{dz} + f(z)y(z) = g(z), \tag{13}$$

with the boundary condition $y(z_o) = y_o$. The solution of the ODE is

$$y(z) = \left[\int_{z_o}^{z} g(z') e^{\int_{z_o}^{z'} f(z'')dz''} dz' + y_o \right] e^{-\int_{z_o}^{z} f(z')dz'}. \tag{14}$$

The zeroth order RT solution

To solve the RT equations for the zeroth order, we first ignore the scattering by assuming $\overline{\overline{P}} = 0$. Thus we obtain

$$\cos\theta \frac{d}{dz} \overline{I}_u^{(0)}(\theta, \phi, z) = -\kappa_e \overline{I}_u^{(0)}(\theta, \phi, z) + \overline{I}_{Tu}(\theta, \phi), \tag{15}$$

$$-\cos\theta \frac{d}{dz} \overline{I}_d^{(0)}(\theta, \phi, z) = -\kappa_e \overline{I}_d^{(0)}(\theta, \phi, z) + \overline{I}_{Td}(\theta, \phi), \tag{16}$$

with the boundary conditions

$$\overline{I}_d^{(0)}(\theta, \phi, d_1) = \overline{I}_d^A(\theta, \phi, d_1), \tag{17}$$

$$\overline{I}_u^{(0)}(\theta, \phi, 0) = 0. \tag{18}$$

From the formula of the general solution (14) of the first order ODE, the zeroth order solutions of the RT equations (9) and (10) can be derived as follows:

$$\overline{I}_u^{(0)}(\theta,\phi,z) = \overline{I}_{Tu}(\theta,\phi)\frac{1-e^{-z\sec\theta\kappa_e}}{\kappa_e}, \tag{19}$$

$$\overline{I}_d^{(0)}(\theta,\phi,z) = \overline{I}_{Td}(\theta,\phi)\frac{1-e^{-(d_1-z)\sec\theta\kappa_e}}{\kappa_e} + \overline{I}_d^A(\theta,\phi,d_1)e^{-(d_1-z)\sec\theta\kappa_e}. \tag{20}$$

The first order RT solution

Plugging the zeroth order solutions (19) and (20) into the RT equations (9) and (10), and defining the terms from the zeroth order solutions as follows:

$$\begin{aligned}\overline{I}_{Tu}^{(1)}(\theta,\phi,z) = & \int\limits_{\text{upper } 2\pi} d\Omega' \overline{\overline{P}}(\theta,\phi,\theta',\phi')\cdot\overline{I}_u^{(0)}(\theta',\phi',z) \\ & + \int\limits_{\text{lower } 2\pi} d\Omega' \overline{\overline{P}}(\theta,\phi,\pi-\theta',\phi')\cdot\overline{I}_d^{(0)}(\theta',\phi',z) \\ & + \overline{I}_{Tu}(\theta,\phi),\end{aligned} \tag{21}$$

$$\begin{aligned}\overline{I}_{Td}^{(1)}(\theta,\phi,z) = & \int\limits_{\text{upper } 2\pi} d\Omega' \overline{\overline{P}}(\pi-\theta,\phi,\theta',\phi')\cdot\overline{I}_u^{(0)}(\theta',\phi',z) \\ & + \int\limits_{\text{lower } 2\pi} d\Omega' \overline{\overline{P}}(\pi-\theta,\phi,\pi-\theta',\phi')\cdot\overline{I}_d^{(0)}(\theta',\phi',z) \\ & + \overline{I}_{Td}(\theta,\phi),\end{aligned} \tag{22}$$

we set up the first order RT equations as

$$\cos\theta\frac{d}{dz}\overline{I}_u^{(1)}(\theta,\phi,z) = -\kappa_e\overline{I}_u^{(1)}(\theta,\phi,z) + \overline{I}_{Tu}^{(1)}(\theta,\phi,z), \tag{23}$$

$$-\cos\theta\frac{d}{dz}\overline{I}_d^{(1)}(\theta,\phi,z) = -\kappa_e\overline{I}_d^{(1)}(\theta,\phi,z) + \overline{I}_{Td}^{(1)}(\theta,\phi,z), \tag{24}$$

with the boundary conditions

$$\overline{I}_d^{(1)}(\theta,\phi,d_1) = \overline{I}_d^A(\theta,\phi,d_1), \tag{25}$$

$$\overline{I}_u^{(1)}(\theta,\phi,0) = 0. \tag{26}$$

Again by using the general solution (14) of the ODE, the solutions of the first order RT equations are obtained as

$$\overline{I}_u^{(1)}(\theta,\phi,z) = \left[\int_0^z \sec\theta\, \overline{I}_{Tu}^{(1)}(\theta,\phi,z')\, e^{z'\sec\theta\kappa_e}\, dz'\right] e^{-z\sec\theta\kappa_e}, \quad (27)$$

$$\begin{aligned}\overline{I}_d^{(1)}(\theta,\phi,z) = \Bigg[&-\sec\theta \int_{d_1}^{z} \overline{I}_{Td}^{(1)}(\theta,\phi,z') e^{-z'\sec\theta\kappa_e} dz' \\ &+\overline{I}_d^{A}(\theta,\phi,d_1) e^{-d_1\sec\theta\kappa_e}\Bigg] e^{z\sec\theta\kappa_e}. \end{aligned} \quad (28)$$

The specific intensity in the foam layer we are interested in is the up-going intensity at $z = d_1$. By integrating over the elevation in Eq. (27), the first order intensity of the up-going wave at the top of the foam layer can be written as

$$\begin{aligned}\overline{I}_u^{(1)}(\theta,\phi,d_1) = {} & \overline{I}_{Tu}(\theta,\phi)\frac{1-e^{-d_1\sec\theta\kappa_e}}{\kappa_e} \\ & +\sec\theta \int_{\text{upper } 2\pi} d\Omega'\, \overline{\overline{P}}(\theta,\phi,\theta',\phi')\cdot \overline{I}_{Tu}(\theta',\phi')\frac{1}{\kappa_e^2} \\ & \left(\frac{1-e^{-d_1\sec\theta\kappa_e}}{\sec\theta} - \frac{e^{-d_1\sec\theta'\kappa_e} - e^{-d_1\sec\theta\kappa_e}}{\sec\theta-\sec\theta'}\right) \\ & +\sec\theta \int_{\text{lower } 2\pi} d\Omega'\, \overline{\overline{P}}(\theta,\phi,\pi-\theta',\phi')\cdot \overline{I}_{Td}(\theta',\phi')\frac{1}{\kappa_e^2} \\ & \left(\frac{1-e^{-d_1\sec\theta\kappa_e}}{\sec\theta} - \frac{1-e^{-d_1(\sec\theta+\sec\theta')\kappa_e}}{\sec\theta+\sec\theta'}\right) \\ & +\sec\theta \int_{\text{lower } 2\pi} d\Omega'\, \overline{\overline{P}}(\theta,\phi,\pi-\theta',\phi')\cdot \overline{I}_d^{A}(\theta',\phi',d_1) \\ & \frac{1-e^{-d_1(\sec\theta+\sec\theta')\kappa_e}}{(\sec\theta+\sec\theta')\kappa_e}. \end{aligned} \quad (29)$$

Assuming $d_1\kappa_e \gg 1$, the Stokes vector of the thick foam layer is given as follows

$$\begin{aligned}\overline{I}_u^{AF}(\theta,\phi,d_1) &\approx \overline{I}_u^{(1)}(\theta,\phi,d_1) \\ &\approx \overline{I}_{Tu}(\theta,\phi)\frac{1}{\kappa_e} + \int_{\text{upper } 2\pi} d\Omega'\, \overline{\overline{P}}(\theta,\phi,\theta',\phi')\cdot \overline{I}_{Tu}(\theta',\phi')\frac{1}{\kappa_e^2}\end{aligned}$$

$$+ \int\limits_{\text{lower } 2\pi} d\Omega' \overline{\overline{P}}(\theta, \phi, \pi - \theta', \phi')$$
$$\cdot \overline{I}_{Td}(\theta', \phi') \frac{1}{\kappa_e^2} \left(1 - \frac{\sec\theta}{\sec\theta + \sec\theta'}\right)$$
$$+ \int\limits_{\text{lower } 2\pi} d\Omega' \overline{\overline{P}}(\theta, \phi, \pi - \theta', \phi')$$
$$\cdot \overline{I}_d^A(\theta', \phi', d_1) \frac{\sec\theta}{(\sec\theta + \sec\theta')\kappa_e}, \tag{30}$$

where the first term denotes the direct emission due to the physical temperature of the foam layer, the second and the third term are the scattering of emission by the scatterers in the foam layer, and the fourth term is the scattering of the atmospheric emission. Notice that the up-going and down-going specific intensities due to the physical temperature in the foam layer are direction independent and they are given by

$$\overline{I}_{Tu}(\theta, \phi) = \overline{I}_{Td}(\theta, \phi) = \bar{\kappa}_a C T_o = \kappa_a C T_o \begin{bmatrix} 1 \\ 1 \\ 0 \\ 0 \end{bmatrix}. \tag{31}$$

2.3. Foam Coverage

Let the foam coverage be F, thus the total brightness temperature is [8]

$$\overline{T}_u^T(\theta, \phi, d_1) = F \cdot \overline{T}_u^{AF}(\theta, \phi, 0) + (1 - F) \cdot \overline{T}_u^{AS}(\theta, \phi, 0), \tag{32}$$

where $\overline{T}_u^{AF}(\theta, \phi, d_1)$ is the emission of the 100% foam as in Eq. (30), and $\overline{T}_u^{AS}(\theta, \phi, 0)$ is the emission of the plain ocean surface with the consideration of the reflection of atmospheric emission that will be discussed in the following sections. Notice that, at this stage, we only consider the emission at the zero elevation height ($z = 0$). We need to consider atmospheric attenuation and radiation if we calculate the total brightness temperature at the height of the radiometer ($z = d_2$). The empirical formula of the foam coverage F as the function of the wind speed U_w, the polar angle θ, and the operating frequency f was

provided by Stogryn [8] and later used by Pandey [9] among others. The foam coverage is expressed as [8]

$$F = b_0 + b_1 U_w + b_2 U_w^2, \tag{33}$$

where the coefficients b_0, b_1 and b_2 are frequency dependent, and they are given by

$$\begin{aligned} b_0 &= 1.707 \times 10^{-2} + 8.560 \times 10^{-4} f + 1.120 \times 10^{-5} f^2, \\ b_1 &= -1.501 \times 10^{-2} + 1.821 \times 10^{-3} f - 4.634 \times 10^{-5} f^2, \\ b_2 &= 2.442 \times 10^{-4} - 2.282 \times 10^{-6} f + 4.194 \times 10^{-7} f^2. \end{aligned} \tag{34}$$

In (33) and (34), the units of the wind speed and the frequency are m/s and GHz, respectively.

3. THERMAL EMISSION FROM PLAIN OCEAN SURFACE

In local regions without foam, the thermal emission from the ocean surface is the sum of the reflection of the atmospheric emission and the thermal emission from the plain ocean surface, i.e.,

$$\overline{I}_u^{AS}(\theta, \phi, 0) = \int\limits_{\text{lower } 2\pi} d\Omega' \, \overline{\overline{R}}(\theta, \phi, \pi - \theta', \phi') \cdot \overline{I}_d^A(\theta', \phi', 0) + \overline{I}_u^S(\theta, \phi, 0), \tag{35}$$

where $\overline{\overline{R}}$ is the reflection matrix of the rough sea surface, $\overline{I}_d^A(\theta', \phi', 0)$ is the thermal emission of the atmosphere, and $\overline{I}_u^S$ is the thermal emission of the plain ocean surface. The details of calculating the atmospheric emission $\overline{I}_d^A(\theta', \phi', 0)$ will be discussed in Section 3.2.

Considering that the ocean water is in thermal equilibrium, the Stokes vector is related to the emissivity $\bar{e}$ by

$$\overline{I}_u^S(\theta, \phi, 0) = \frac{K_B}{\lambda^2} \bar{e}(\theta, \phi) T_s, \tag{36}$$

where T_s is the physical temperature of the rough ocean surface. By Kirchhoff's law, the emissivity vector $\bar{e}(\theta, \phi)$ is the intensity of incident wave with unit amplitude minus the total intensity of the reflected waves,

$$\bar{e}(\theta, \phi) = \overline{I}_i - \int \overline{I}_r(\theta, \phi; \theta_i, \phi_i; 0) d\Omega_i, \tag{37}$$

where

$$\overline{I}_i = \frac{1}{\eta} \begin{bmatrix} \langle |E_{vi}|^2 \rangle \\ \langle |E_{hi}|^2 \rangle \\ 2\mathrm{Re}\langle E_{vi} E_{hi}^* \rangle \\ 2\mathrm{Im}\langle E_{vi} E_{hi}^* \rangle \end{bmatrix} = \begin{bmatrix} 1 \\ 1 \\ 0 \\ 0 \end{bmatrix}. \tag{38}$$

The amplitude of the v and h-polarized incident electric fields is unity, and $\overline{I}_r$ is the reflection Stokes vector of the plane wave with incident angles θ_i and ϕ_i.

3.1. Stokes Vector of Reflected Wave

We apply the small perturbation method (SPM) to calculate the reflection matrix $\overline{\overline{R}}$ of the rough surface and then calculate the reflection Stokes vector $\overline{I}_r$. The reflection Stokes vector can be written as

$$\overline{I}_r(\theta, \phi, \theta_i, \phi_i; 0) = \overline{\overline{R}}(\theta, \phi, \theta_i, \phi_i) \cdot \overline{I}_i(\theta_i, \phi_i; 0), \tag{39}$$

where $\overline{\overline{R}}$ is the reflection matrix for the Stokes vector.

In the zeroth order SPM solution, the scattered field is specular and is equivalent to the flat-surface scattering problem; thus the reflection coefficients of the zeroth order solution are the Fresnel reflection coefficients. Using the ensemble average, the second order solution from SPM is also specular. Therefore we call both the zeroth and second-order terms coherent. The averaged field of the first order solution by SPM is zero, hence it is incoherent. By including solutions up to the second order using SPM, the reflection matrix is the sum of coherent and incoherent parts, $\overline{\overline{R}}^c$ and $\overline{\overline{R}}^i$, respectively, so that

$$\overline{\overline{R}} = \overline{\overline{R}}^c + \overline{\overline{R}}^i. \tag{40}$$

Since the scattered field from the zeroth and second order SPM solutions is specular, the coherent reflection matrix of the Stokes vector can be written as

$$\overline{\overline{R}}^c(\theta, \phi, \pi - \theta_i, \phi_i) = \left[R_{ij}^c\right] \delta(\cos\theta - \cos\theta_i)\delta(\phi - \phi_i)$$

$$= \begin{bmatrix} R_{11}^c & R_{12}^c & R_{13}^c & R_{14}^c \\ R_{21}^c & R_{22}^c & R_{23}^c & R_{24}^c \\ R_{31}^c & R_{32}^c & R_{33}^c & R_{34}^c \\ R_{41}^c & R_{42}^c & R_{43}^c & R_{44}^c \end{bmatrix} \delta(\cos\theta - \cos\theta_i)\delta(\phi - \phi_i). \quad (41)$$

Note that the subscripts i and j are associated with the scattered and incident components of the Stokes vector, respectively. The element R_{ij}^c $(i, j = 1, 2, 3, 4)$ is related to the reflection coefficient $R_{\alpha\beta}$ with subscripts $\alpha, \beta = v, h$, where

$$\begin{bmatrix} E_{vs}^c \\ E_{hs}^c \end{bmatrix} = \begin{bmatrix} R_{vv}^c(\theta_i, \phi_i) & R_{vh}^c(\theta_i, \phi_i) \\ R_{hv}^c(\theta_i, \phi_i) & R_{hh}^c(\theta_i, \phi_i) \end{bmatrix} \begin{bmatrix} E_{vi} \\ E_{hi} \end{bmatrix}, \quad (42)$$

and the subscripts v and h represent vertically and horizontally polarized waves, respectively. By writing

$$\overline{I}_u^c = \frac{1}{\eta} \begin{bmatrix} |E_{vs}^c|^2 \\ |E_{hs}^c|^2 \\ 2\mathrm{Re}\{E_{vs}^c E_{hs}^{c*}\} \\ 2\mathrm{Im}\{E_{vs}^c E_{hs}^{c*}\} \end{bmatrix}$$

and expressing E_{vs}^c and E_{hs}^c in terms of E_{vi}^c and E_{hi}^c using Eq. (42), it can be shown that

$$\overline{I}_u^c = \left[R_{ij}^c\right] \cdot \overline{I}_i, \quad (43)$$

where

$$\left[R_{ij}^c\right] = \begin{bmatrix} |R_{vv}^c|^2 & |R_{vh}^c|^2 & \mathrm{Re}(R_{vv}^c R_{vh}^{*c}) & -\mathrm{Im}(R_{vv}^c R_{vh}^{*c}) \\ |R_{hv}^c|^2 & |R_{hh}^c|^2 & \mathrm{Re}(R_{hv}^c R_{hh}^{*c}) & -\mathrm{Im}(R_{hv}^c R_{hh}^{*c}) \\ 2\mathrm{Re}(R_{vv}^c R_{hv}^{*c}) & 2\mathrm{Re}(R_{vh}^c R_{hh}^{*c}) & \mathrm{Re}(R_{vv}^c R_{hh}^{*c} + R_{vh}^c R_{hv}^{*c}) & -\mathrm{Im}(R_{vv}^c R_{hh}^{*c} - R_{vh}^c R_{hv}^{*c}) \\ 2\mathrm{Im}(R_{vv}^c R_{hv}^{*c}) & 2\mathrm{Im}(R_{vh}^c R_{hh}^{*c}) & \mathrm{Im}(R_{vv}^c R_{hh}^{*c} + R_{vh}^c R_{hv}^{*c}) & \mathrm{Re}(R_{vv}^c R_{hh}^{*c} - R_{vh}^c R_{hv}^{*c}) \end{bmatrix} \quad (44)$$

and the incident Stokes vector $\overline{I}_i$ is defined as in Eq. (38). Using SPM, $R^c_{\alpha\beta}$ $(\alpha, \beta = v, h)$ can be obtained as

$$R^c_{\alpha\beta} = \begin{bmatrix} R^{(0)}_{vv} + R^{(2)}_{vv} & R^{(0)}_{vh} + R^{(2)}_{vh} \\ R^{(0)}_{hv} + R^{(2)}_{hv} & R^{(0)}_{hh} + R^{(2)}_{hh} \end{bmatrix}, \tag{45}$$

where the zeroth order $R^{(0)}_{\alpha\beta}$ is the Fresnel reflection coefficient of a flat surface, which is given by

$$\begin{cases} R^{(0)}_{vv} = \dfrac{\epsilon_2 k_{1z} - \epsilon_1 k_{2z}}{\epsilon_2 k_{1z} + \epsilon_1 k_{2z}}, \\ R^{(0)}_{hh} = \dfrac{k_{1z} - k_{2z}}{k_{1z} + k_{2z}}, \\ R^{(0)}_{vh} = R^{(0)}_{hv} = 0. \end{cases} \tag{46}$$

The second order reflection coefficient $R^{(2)}_{\alpha\beta}$ is given by

$$R^{(2)}_{\alpha\beta} = \int_{-\infty}^{\infty} \int_{-\infty}^{\infty} dk_x dk_y W(k_{xi} - k_x, k_{yi} - k_y) f^{(2)}_{\alpha\beta}, \tag{47}$$

where $W(k_{xi} - k_x, k_{yi} - k_y)$ is the spectral density function of the rough ocean surface, and $f^{(2)}_{\alpha\beta}$ is the second-order scattering coefficient as in [1].

The incoherent reflection matrix $\overline{\overline{R}}^i(\theta, \phi; \theta_i, \phi_i)$ can be calculated by considering the first order SPM solution. By expressing the scattering fields as

$$\begin{bmatrix} E_{vs} \\ E_{hs} \end{bmatrix} = \frac{e^{ik_1 r}}{r} \begin{bmatrix} f_{vv}(\theta, \phi; \theta_i, \phi_i) & f_{vh}(\theta, \phi; \theta_i, \phi_i) \\ f_{hv}(\theta, \phi; \theta_i, \phi_i) & f_{hh}(\theta, \phi; \theta_i, \phi_i) \end{bmatrix} \begin{bmatrix} E_{vi} \\ E_{hi} \end{bmatrix}, \tag{48}$$

where $f_{\alpha\beta}(\theta, \phi; \theta_i, \phi_i)$ is the polarimetric scattering coefficient $(\alpha, \beta = h, v)$, the reflection matrix can be calculated by [16]

$$\overline{\overline{R}}^i = \frac{1}{A \cos\theta} \overline{\overline{L}}^i, \tag{49}$$

where

$$\overline{\overline{L}}^{i}(\theta,\phi;\theta_i,\phi_i) = \begin{bmatrix} \left\langle |f_{vv}|^2 \right\rangle & \left\langle |f_{vh}|^2 \right\rangle & \mathrm{Re}\langle (f_{vv}f_{vh}^*)\rangle & -\mathrm{Im}\langle (f_{vv}f_{vh}^*)\rangle \\ \left\langle |f_{hv}|^2 \right\rangle & \left\langle |f_{hh}|^2 \right\rangle & \mathrm{Re}\langle (f_{hv}f_{hh}^*)\rangle & -\mathrm{Im}\langle (f_{hv}f_{hh}^*)\rangle \\ 2\mathrm{Re}\langle (f_{vv}f_{hv}^*)\rangle & 2\mathrm{Re}\langle (f_{vh}f_{hh}^*)\rangle & \mathrm{Re}\langle (f_{vv}f_{hh}^* + f_{vh}f_{hv}^*)\rangle & -\mathrm{Im}\langle (f_{vv}f_{hh}^* - f_{vh}f_{hv}^*)\rangle \\ 2\mathrm{Im}\langle (f_{vv}f_{hv}^*)\rangle & 2\mathrm{Im}\langle (f_{vh}f_{hh}^*)\rangle & \mathrm{Im}\langle (f_{vv}f_{hh}^* + f_{vh}f_{hv}^*)\rangle & \mathrm{Re}\langle (f_{vv}f_{hh}^* - f_{vh}f_{hv}^*)\rangle \end{bmatrix}. \tag{50}$$

and A is the illuminated area. The ensemble averaged product of the scattering coefficients is related to the polarimetric bistatic scattering coefficient as following:

$$\gamma^{i}_{\alpha\beta\mu\nu}(\theta,\phi;\theta_i,\phi_i) = \frac{4\pi \left\langle f_{\alpha\beta}(\theta,\phi;\theta_i,\phi_i) f^*_{\mu\nu}(\theta,\phi;\theta_i,\phi_i) \right\rangle}{A\cos\theta_i}. \tag{51}$$

From expression (49), (50) and (51), it can be easily derived that

$$\overline{\overline{R}}^{i} = \frac{\cos\theta_i}{4\pi\cos\theta} \begin{bmatrix} \gamma^i_{vvvv} & \gamma^i_{vhvh} & \mathrm{Re}\gamma^i_{vvvh} & -\mathrm{Im}\gamma^i_{vvvh} \\ \gamma^i_{hvhv} & \gamma^i_{hhhh} & \mathrm{Re}\gamma^i_{hvhh} & -\mathrm{Im}\gamma^i_{hvhh} \\ 2\mathrm{Re}\gamma^i_{vvhv} & 2\mathrm{Re}\gamma^i_{vhhh} & \mathrm{Re}\left(\gamma^i_{vvhh} + \gamma^i_{vhhv}\right) & -\mathrm{Im}\left(\gamma^{i*}_{vvhh} - \gamma^i_{vhhv}\right) \\ 2\mathrm{Im}\gamma^i_{vvhv} & 2\mathrm{Im}\gamma^i_{vhhh} & \mathrm{Im}\left(\gamma^i_{vvhh} + \gamma^i_{vhhv}\right) & \mathrm{Re}\left(\gamma^{i*}_{vvhh} - \gamma^i_{vhhv}\right) \end{bmatrix} \tag{52}$$

with

$$\gamma^{i}_{\alpha\beta\mu\nu}(\theta,\phi;\theta_i,\phi_i) = \frac{4\pi k_1^2\cos^2\theta\Gamma_{\alpha\beta\mu\nu}(\theta,\phi;\theta_i,\phi_i)W(\theta,\phi;\theta_i,\phi_i)}{\cos\theta_i}, \tag{53}$$

where $\Gamma_{\alpha\beta\mu\nu}$ is the coefficient with explicit form given in [1]. Finally, by knowing the coherent reflection matrix $\overline{\overline{R}}^{c}$ from Eq. (41) and the incoherent reflection matrix $\overline{\overline{R}}^{i}$ from Eq. (52), we obtain the total reflection $\overline{\overline{R}} = \overline{\overline{R}}^{c} + \overline{\overline{R}}^{i}$ [Eq. (40)]. Therefore the reflection Stokes vector $\overline{I}_r$ is obtained as

$$\overline{I}_r(\theta,\phi,\theta_i,\phi_i;0) = \left(\overline{\overline{R}}^{c} + \overline{\overline{R}}^{i}\right)\cdot\overline{I}_i, \tag{54}$$

and the emissivity can be calculated from Eq. (37) as

$$\begin{aligned}\bar{e}(\theta,\phi) &= \overline{I}_i - \int \left(\overline{\overline{R}}^c + \overline{\overline{R}}^i\right)\cdot \overline{I}_i d\Omega_i \\ &= \overline{I}_i - \int_0^{\pi/2} \sin\theta_i d\theta_i \int_0^{2\pi} d\phi_i \left(\overline{\overline{R}}^c + \overline{\overline{R}}^i\right)\cdot \overline{I}_i. \end{aligned} \tag{55}$$

3.2. Reflection of Atmospheric Thermal Emission

We write the term representing the reflection of the atmospheric thermal emission from the rough surface as

$$\overline{I}_r^A(\theta,\phi;0) = \int d\Omega' \,\overline{\overline{R}}(\theta,\phi,\pi-\theta',\phi')\cdot \overline{I}_d^A(\theta',\phi';0). \tag{56}$$

From Eq. (40) we know that the reflection of the rough surface can be written as the sum of the coherent and incoherent parts, therefore

$$\overline{I}_r^A(\theta,\phi;0) = \int d\Omega' \left(\overline{\overline{R}}^c + \overline{\overline{R}}^i\right)\cdot \overline{I}_d^A(\theta',\phi';0). \tag{57}$$

Thus the total Stokes vector in Eq. (35) can be written as

$$\begin{aligned}\overline{I}_u^{AS}(\theta,\phi;0) &= \int d\Omega' \left(\overline{\overline{R}}^c + \overline{\overline{R}}^i\right)\cdot \overline{I}_d^A(\theta',\phi';0) \\ &\quad + \frac{K_B}{\lambda^2} T_s \left[\overline{I}_i - \int d\Omega_i \left(\overline{\overline{R}}^c + \overline{\overline{R}}^i\right)\cdot \overline{I}_i\right]. \end{aligned} \tag{58}$$

Noticing that $d\Omega' = d\Omega_i$ for the down-going Stokes vector from the atmospheric layer, therefore it can be shown that

$$\begin{aligned}\overline{I}_u^{AS}(\theta,\phi;0) &= \frac{K_B}{\lambda^2} T_s \overline{I}_i - \frac{K_B}{\lambda^2} T_s \int d\Omega_i \left(\overline{\overline{R}}^c + \overline{\overline{R}}^i\right) \\ &\quad \cdot \left[\overline{I}_i - \frac{\lambda^2}{K_B T_s} \overline{I}_d^A(\theta_i,\phi_i;0)\right]. \end{aligned} \tag{59}$$

Converting the Stokes vector to the brightness temperature, the brightness temperature of the plain ocean surface can be written as

$$\begin{aligned}\overline{T}_u^{AS}(\theta,\phi;0) &= \frac{\lambda^2}{K_B} \overline{I}_u^{AS}(\theta,\phi;0) \\ &= \overline{T}_i - \int d\Omega_i \left(\overline{\overline{R}}^c + \overline{\overline{R}}^i\right)\cdot \left[\overline{T}_i - \overline{T}_d^A(\theta_i,\phi_i;0)\right], \end{aligned} \tag{60}$$

where $\overline{T}_i = T_s \overline{I}_i$, and $\overline{T}_d^A(\theta_i, \phi_i; 0) = \dfrac{\lambda^2}{K_B} \overline{I}_d^A(\theta_i, \phi_i; 0)$ is the down-going brightness temperature of the atmosphere at the ocean surface. The down-going specific intensity $\overline{I}_d^A(\theta_i, \phi_i; 0)$ from the atmosphere can be found from Eq. (77) and its approximation can be found in Eq. (89) as

$$\begin{aligned} \overline{I}_d^A(\theta, \phi, d_1) &= \sec\theta \int_{d_1}^{d_2} \bar{\kappa}_a(z') CT(z') e^{-\sec\theta \int_{d_1}^{z'} \kappa_a(z'')dz''} dz' \\ &\approx CT(z_o) \frac{\bar{\kappa}_a}{\kappa_a} \left[1 - e^{-\sec\theta \int_{d_1}^{d_2} \kappa_a(z'')dz''} \right], \end{aligned} \tag{61}$$

where $T(z')$ is the temperature profile of the atmosphere, and κ_a is the absorption coefficient. The median elevation z_o can be calculated by solving the following equation:

$$\int_{d_1}^{z_o} \kappa_a(z')dz' = \frac{1}{2} \int_{d_1}^{d_2} \kappa_a(z')dz'. \tag{62}$$

3.3. Power Spectrum of Rough Ocean Surface

The ocean surface spectrum applied in this thesis was proposed by Durden and Vesecky [17]. This surface spectrum is based on experimental data fitting and thus it is an empirical model. The Durden-Vesecky surface spectrum is given by

$$W(k, \phi) = \frac{a_0}{2\pi k^4} \Phi(k, \phi) S(k), \tag{63}$$

where

$$\Phi(k, \phi) = \left(1 + c(1 - e^{-sk^2}) \cos 2\phi\right), \tag{64}$$

$$S(k) = \begin{cases} e^{-0.74\left(\frac{g}{U_{19.5}^2 k}\right)^2} & \text{if } 0 < k < 2, \\ \left(\frac{bku_*^2}{g + \gamma k^2}\right)^{a \log_{10}(k/2)} & \text{if } k > 2. \end{cases} \tag{65}$$

The wind friction velocity u_* can be found from the following equation

$$U_h = \frac{u_*}{0.4} \log \frac{h}{6.84 \times 10^{-5}/u_* + 4.28 \times 10^{-3} u_*^2 - 4.43 \times 10^{-4}}, \tag{66}$$

where U_h is the wind speed in the unit of m/s at the elevation height h in meters above the mean ocean surface. k is the ocean surface spatial wavenumber, ϕ is the azimuthal angle with respect to wind direction, a_0, a, b, g, γ, and s are constants with the values of $a_0 = 0.008$, $a = 0.225$, $b = 1.25$, $g = 9.81$, $\gamma = 7.25 \times 10^{-5}$, $s = 1.5 \times 10^{-4}$. The parameter c, which serves as the coefficient for the azimuthal-dependent term in the spectrum, is given by

$$c = \frac{2(1-R)/(1+R)}{1-D}, \tag{67}$$

where

$$R = \frac{0.003 + 1.92 \times 10^{-3} U_{12.5}}{3.16 \times 10^{-3} U_{12.5},} \tag{68}$$

$$D = \frac{\int_0^\infty dk\, k^2\, S(k)\, e^{-(k/89.44)^2}}{\int_0^\infty dk\, k^2\, S(k)}. \tag{69}$$

For example, for the wind speed $U_h = 12$ m/s at height $h = 19.5$ m, it can be calculated that $u_* = 0.46388$ and $c = 0.65139$. To consider certain hydrodynamic effects of the ocean waves, we multiply the parameter c in the spectrum density function $W(k, \phi)$ by $(1 - d_0 \cos\phi)$, where the parameter d_0 is determined by data matching. The hydrodynamic modulation was also modeled differently by multiplying the ocean surface spectrum with a parameter h' based on the slope of the long waves [17, 18]. The modulated spectrum is written as

$$W(k, \phi, S_x) = h'\, W(k, \phi), \tag{70}$$

where S_x is the slope of the large-scale waves on the ocean surface and h' is calculated as

$$h' = \begin{cases} 1 - 0.5\,\mathrm{sgn}(S_x) & \text{if } |S_x/S_u| > 1.25, \\ 1 - 0.4\, S_x/S_u & \text{if } |S_x/S_u| \le 1.25, \end{cases} \tag{71}$$

where S_u is the rms upwind surface slope which can be calculated by using Eq. (110). The hydrodynamic modulation of the ocean surface spectrum using the parameter h' is useful for the two-scale model of the ocean surface. A detailed study can be found in Section 5.

4. RADIATIVE TRANSFER EQUATIONS FOR ATMOSPHERE

The atmospheric contribution to the brightness temperature of the ocean surface must be taken into account since (1) the airborne radiometer is usually at a very high altitude, hence the accumulated thermal emission along the path from the ocean surface to the radiometer may be significant, and/or the attenuation for the brightness temperature propagating from the ocean surface up to the radiometer cannot be negligible, and (2) there may be a significant amount of down-going thermal emission from the atmosphere being reflected by the ocean surface. In clear air conditions, the main concerns about the atmosphere for passive remote sensing are the atmospheric emission and attenuation due to the contributions from gaseous oxygen (O_2), water vapor (H_2O), and suspended water droplets (hydrosols) [19]. In the adverse conditions, cloud and rainfall need to be addressed [19,20]. In clear air and at microwave frequencies, the electromagnetic wave scattering by atmospheric gases can be ignored [21], thus the radiative transfer (RT) equations that are used to model the wave propagation in the atmosphere reduce to uncoupled first-order differential equations.

The atmosphere can be modeled as an inhomogeneous layer with the extinction coefficient $\kappa_e(z)$, the absorption coefficient $\kappa_a(z)$, and the temperature profile $T(z)$ in terms of the height z as shown in Fig. 3. We assume that the scatterers such as water vapor, droplets and gaseous oxygen are small thus the scattering is ignored ($\kappa_e = \kappa_s + \kappa_a \approx \kappa_a$). Therefore the radiative transfer equations for the specific intensity $\overline{I}_u^A$ and $\overline{I}_d^A$ have the following simple form [15, 22]

$$\cos\theta \frac{\partial}{\partial z}\overline{I}_u^A(\theta,\phi,z) = -\kappa_a(z)\overline{I}_u^A(\theta,\phi,z) + \bar{\kappa}_a CT(z), \tag{72}$$

$$-\cos\theta \frac{\partial}{\partial z}\overline{I}_d^A(\theta,\phi,z) = -\kappa_a(z)\overline{I}_d^A(\theta,\phi,z) + \bar{\kappa}_a CT(z), \tag{73}$$

where $C = K_B/\lambda^2$, K_B is Boltzmann constant and λ is the electromagnetic wavelength.

Assuming that there is no thermal emission from the upper space at $z = d_2$, the boundary conditions for Eqs. (72) and (73) are given by

$$\overline{I}_u^A(\theta,\phi,d_1) = \overline{I}_u^T(\theta,\phi,d_1), \tag{74}$$

$$\overline{I}_d^A(\theta,\phi,d_2) = 0, \tag{75}$$

where $\overline{I}_u^T(\theta,\phi,d_1)$ denotes the emission from the lower boundary at $z = d_1$ (the foam-covered ocean surface). From Eq. (14), the solution

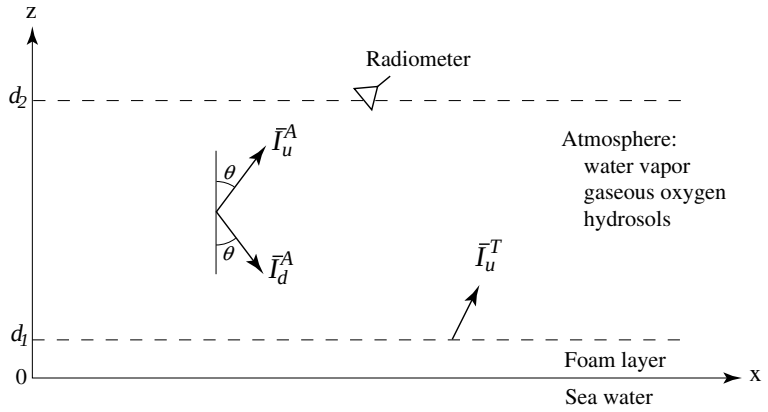

Figure 3. The atmospheric layer above a foam-covered ocean surface.

of the RT equations (72) and (73) are obtained as

$$\overline{I}_u^A(\theta,\phi,d_2) = \sec\theta \int_{d_1}^{d_2} \bar{\kappa}_a(z')CT(z')\, e^{-\sec\theta \int_{z'}^{d_2} \kappa_a(z'')dz''} dz' + \overline{I}_u^T(\theta,\phi,d_1)\, e^{-\sec\theta \int_{d_1}^{d_2} \kappa_a(z')dz'}, \quad (76)$$

$$\overline{I}_d^A(\theta,\phi,d_1) = \sec\theta \int_{d_1}^{d_2} \bar{\kappa}_a(z')CT(z')\, e^{-\sec\theta \int_{d_1}^{z'} \kappa_a(z'')dz''} dz'. \quad (77)$$

The specific intensity of the down-going wave in Eq. (77) can be calculated for any polar angle θ from the absorption and temperature profiles. From the equation of the down-going wave in Eq. (77) we find that the assumption that down-going wave at height d_2 is zero as in Eq. (75) is due to the fact that the absorption coefficient κ_a at $z = d_2$ is very small. In the next sections, we will see from the numerical results for the US Standard Atmosphere [23] that the value of the absorption coefficient is negligible for altitude larger than 10 km. In the RT theory, if the scattering is ignored for the propagating wave, the absorption coefficient κ_a is two times the imaginary part of the complex wavenumber,

$$\kappa_a = 2\mathrm{Im}\{k\} = 2\mathrm{Im}\left\{(10^{-6}N + 1)k_o\right\}, \quad (78)$$

where k_o is the wavenumber in free space, and N is the complex refractivity. In the following sections, we will use Liebe's millimeter-wave propagation model (MPM) [24] to calculate the complex refractivity in the atmosphere.

The extinction coefficient κ_e is the sum of the scattering coefficient κ_s and the absorption coefficient of the background κ_a. Quantitatively, we find that $\kappa_s \ll \kappa_a$,therefore we use κ_a to approximate κ_e. The dominant scattering in the atmosphere is due to water vapor and suspended water droplets (hydrosols). The scattering and absorption coefficient are given by [15, page 157–158]

$$\kappa_s = 2f_v k^4 a^3 |y|^2, \tag{79}$$

$$\kappa_a = f_v k \frac{\epsilon_s''}{\epsilon} \left| \frac{3\epsilon}{\epsilon_s + 2\epsilon} \right|^2, \tag{80}$$

where f_v is the fractional volume occupied by the water particles, a is the radius of a water particle, and

$$y = \frac{\epsilon_s - \epsilon}{\epsilon_s + 2\epsilon}. \tag{81}$$

For water droplets in the atmosphere, the typical values are $a \sim 5$ μm, $f_v \sim 5 \times 10^{-7}$, and $\epsilon_s \sim 30 + i40$ for $f = 20$ GHz. Therefore $\kappa_s \sim 10^{-12}$ m^{-1} and $\kappa_a \sim 10^{-5}$ m^{-1}, thus $\kappa_s \ll \kappa_a$ and we can ignore κ_s and let $\kappa_e \approx \kappa_a$. The gaseous oxygen ($O_2$), water vapor ($H_2O$), and suspended water droplets in the atmosphere are considered as the principal absorbers in moist air [19].

4.1. The Millimeter-Wave Propagation Model

The millimeter-wave propagation model (MPM) model developed by Liebe [24] can be used to calculate the complex refractivity N that is related to the complex refractive index n by $N = 10^6(n-1)$. By writing the refractive index as $n = n' + in''$, the effective permittivity of moist air is found as following:

$$\epsilon_e = (n' + in'')^2 = \left(n'^2 - n''^2\right) + i(2n'n''), \tag{82}$$

where k_o is the wavenumber in free space. Thus the complex wavenumber is given by

$$k = \omega\sqrt{\mu_e \epsilon_e} = k_o n, \tag{83}$$

assuming $\mu_e = \mu_o$. The measurable parameters of atmosphere are (1) barometric pressure P in kilopascal (1 kPa = 10 mbar), (2) temperature T in degrees Kelvin (K), (3) relative humidity RH, and (4)

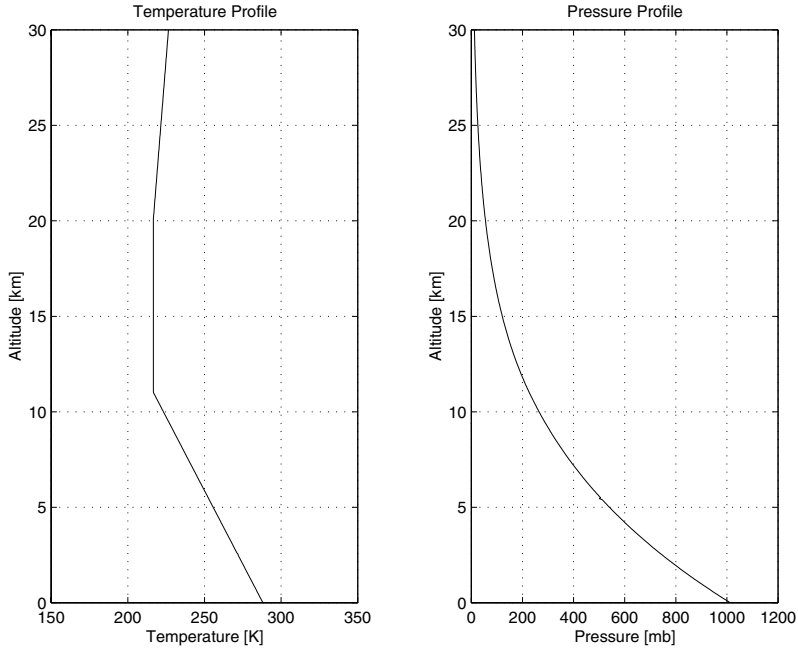

Figure 4. Temperature and barometric pressure profiles in the US Standard Atmosphere 1976.

mass concentration in grams per cubic meter. The four measurable parameters can be converted to the internal variables which are useful in the MPM model as shown in Appendix B.

The typical barometric pressure profile is given in [23] and it is plotted in Fig. 4. As an example, we consider the frequency $f = 19.35$ GHz and use the US Standard Atmosphere 1976 temperature, barometric pressure and humidity profiles to calculate the complex wavenumber k for an electromagnetic wave propagating in the atmosphere. The numerical result of the absorption coefficient is plotted in Fig. 5, where the real and imaginary parts are plotted separately in terms of the wavenumber in free space k_o.

4.2. Attenuation and Emission of Atmosphere

Once we obtained the key parameter — the absorption coefficient κ_a from the MPM model, the thermal emission of the standard atmosphere and its attenuation for the propagating waves can be calculated by using the RT solutions (76) and (77). The first term in

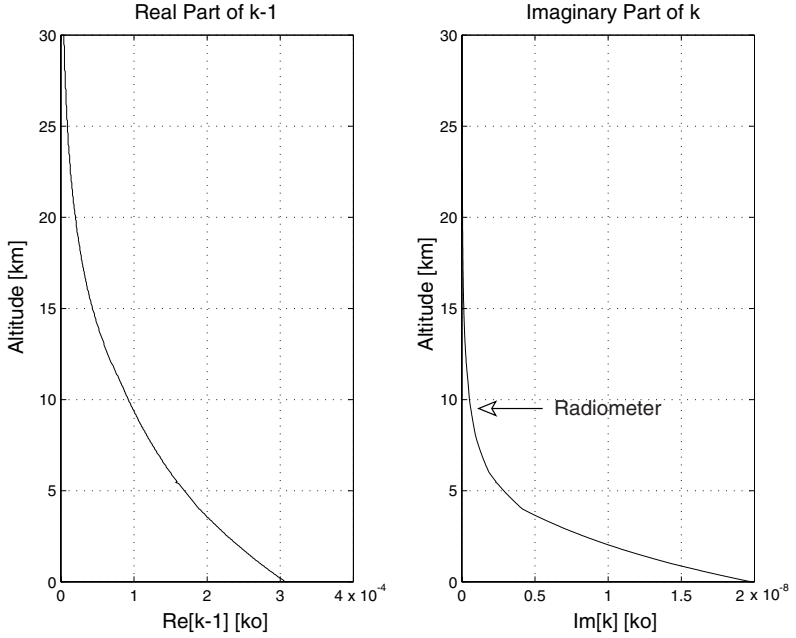

Figure 5. The complex wavenumber of electromagnetic wave with $f = 19.35$ GHz propagating in the atmosphere in terms of the wavenumber in free space.

Eq. (76) represents the up-going thermal emission of the atmosphere and can be written as

$$\overline{I}^A_{u1}(\theta,\phi,d_2) = \sec\theta \int_{d_1}^{d_2} \bar{\kappa}_a(z')CT(z')e^{-\sec\theta \int_{z'}^{d_2} \kappa_a(z'')dz''} dz'. \tag{84}$$

The down-going wave in Eq. (77) represents the down-going thermal emission of the atmosphere,

$$\overline{I}^A_{d}(\theta,\phi,d_1) = \sec\theta \int_{d_1}^{d_2} \bar{\kappa}_a(z')CT(z')e^{-\sec\theta \int_{d_1}^{z'} \kappa_a(z'')dz''} dz'. \tag{85}$$

The up and down-going thermal emissions can be calculated using the result of absorption and temperature profiles from the MPM. We can show numerically that they are very close to each other quantitatively.

The up-going thermal emission as in Eq. (84) can be written as

$$\overline{I}_{u1}^{A}(\theta,\phi,d_2) = CT(z_o)\sec\theta \int_{d_1}^{d_2} \bar{\kappa}_a(z') e^{-\sec\theta \int_{z'}^{d_2} \kappa_a(z'')dz''} dz', \tag{86}$$

where z_o is between d_1 and d_2. The down-going wave as in Eq. (85) can also be written as

$$\overline{I}_{d}^{A}(\theta,\phi,d_1) = CT(z_o')\sec\theta \int_{d_1}^{d_2} \bar{\kappa}_a(z') e^{-\sec\theta \int_{d_1}^{z'} \kappa_a(z'')dz''} dz', \tag{87}$$

where z_o' is between d_1 and d_2 but different from z_o. It can be shown that

$$\begin{aligned}\int_{d_1}^{d_2} \kappa_a(z') e^{-\sec\theta \int_{z'}^{d_2} \kappa_a(z'')dz''} dz' &= \int_{d_1}^{d_2} \kappa_a(z') e^{-\sec\theta \int_{d_1}^{z'} \kappa_a(z'')dz''} dz' \\ &= \cos\theta \left[1 - e^{-\sec\theta \int_{d_1}^{d_2} \kappa_a(z'')dz''}\right]. \end{aligned} \tag{88}$$

Since the temperature profile $T(z)$ does not change much for the entire integral path, i.e., $T(z_o) \approx T(z_o')$,

$$\overline{I}_{u1}^{A}(\theta,\phi,d_2) \approx \overline{I}_{d}^{A}(\theta,\phi,d_1) \approx CT(z_o)\,\frac{\bar{\kappa}_a}{\kappa_a}\left[1 - e^{-\sec\theta \int_{d_1}^{d_2} \kappa_a(z'')dz''}\right], \tag{89}$$

where z_o is the median elevation as defined in Eq. (62). Figure 6 shows the numerical result of the down-going, up-going and approximated brightness temperatures by carrying out the integration for Eqs. (84) and (85) numerically or using approximation formula Eq. (89) for the standard atmosphere at $f = 19.35$ GHz, $d_2 = 30$ km and $d_1 = 0$.

In the second term of the up-going wave in Eq. (76), the factor

$$\exp\left(-\sec\theta \int_{d_1}^{d_2} \kappa_a(z')dz'\right)$$

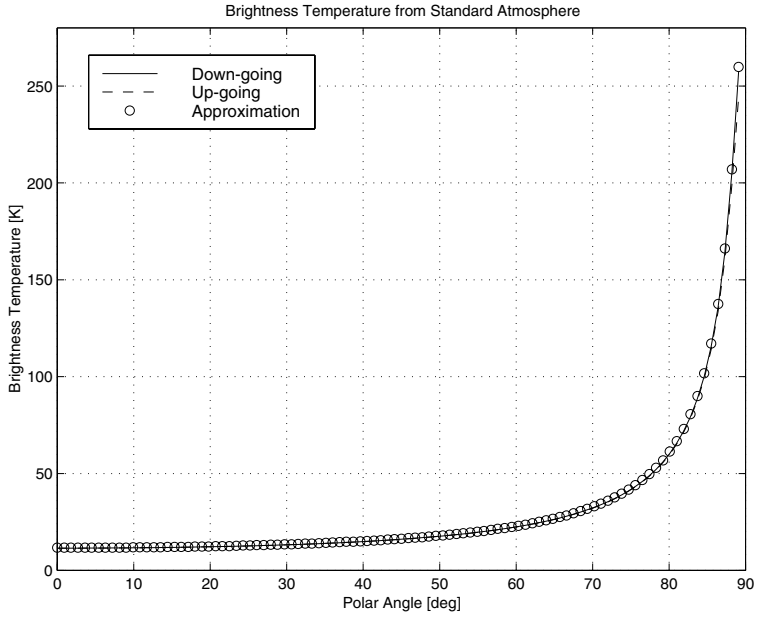

Figure 6. The brightness temperature of down-going and up-going waves and their comparison with the approximation formula for $f = 19.35$ GHz.

is the attenuation for the thermal emission from the foam-covered ocean surface. For the US standard atmosphere at $f = 19.35$ GHz, $d_2 = 30$ km and $d_1 = 0$, we can calculate the attenuation using the numerical κ_a from the MPM. Fig. 7 shows the attenuation in terms of the polar angle.

After the total brightness temperature on the ocean surface is calculated by [also from Eq. (32)]

$$\overline{T}_u^T(\theta, \phi, d_1) = F \cdot \overline{T}_u^{AF}(\theta, \phi, d_1) + (1 - F) \cdot \overline{T}_u^{AS}(\theta, \phi, 0), \qquad (90)$$

we can calculate the brightness temperature at the height of the radiometer. Between the ocean surface and the radiometer, the atmospheric emission and the attenuation must be taken into account. At the radiometer height $z = d_2$, by dividing the constant $C = K_B/\lambda^2$ on both sides of Eq. (76), the total brightness temperature can be

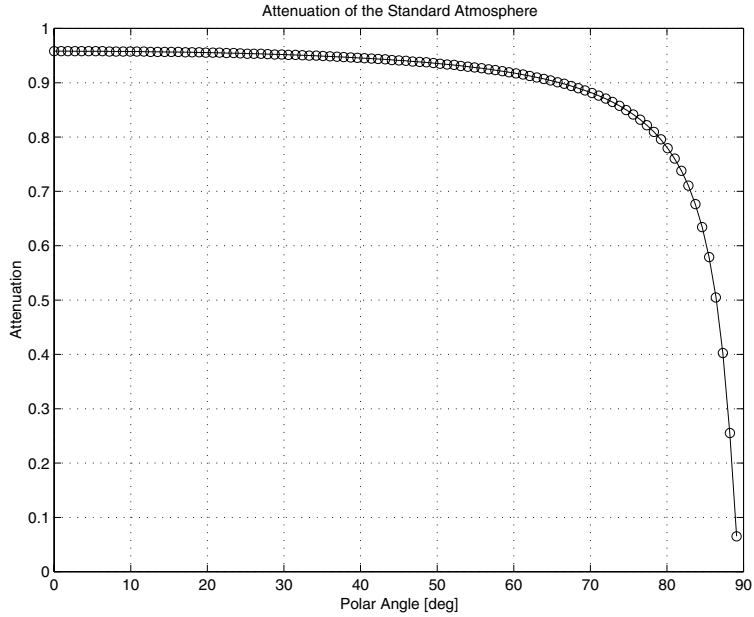

Figure 7. The attenuation of the standard atmosphere for $f = 19.35$ GHz, $d_2 = 30$ km and $d_1 = 0$.

written as

$$\overline{T}_u^A(\theta,\phi,d_2) \;=\; \sec\theta \int_{d_1}^{d_2} \bar{\kappa}_a(z')T(z')e^{-\sec\theta \int_{z'}^{d_2} \kappa_a(z'')dz''} dz' + \overline{T}_u^T(\theta,\phi,d_1)e^{-\sec\theta \int_{d_1}^{d_2} \kappa_a(z')dz'}, \tag{91}$$

where the first term is the thermal emission of the atmosphere and the exponential factor in the second term is the atmospheric attenuation for the wave traveling from the ocean surface to the radiometer. In order to study individually the contributions from the plain ocean surface, the foam and the atmosphere, we re-label the terms in Eq. (90) and Eq. (91) as

$$\overline{T}_S \;=\; (1-F)\cdot \overline{T}_u^{AS}(\theta,\phi,0)e^{-\sec\theta \int_0^{d_2} \kappa_a(z')dz'}, \tag{92}$$

$$\overline{T}_F = F \cdot \overline{T}_u^{AF}(\theta, \phi, d_1) e^{-\sec\theta \int_{d_1}^{d_2} \kappa_a(z')dz'}, \tag{93}$$

$$\overline{T}_A = \sec\theta \int_{d_1}^{d_2} \bar{\kappa}_a(z') T(z') e^{-\sec\theta \int_{z'}^{d_2} \kappa_a(z'')dz''} dz'. \tag{94}$$

In the above expressions, $\overline{T}_S$ is the brightness temperature of the plain ocean surface with the consideration of reflection of atmospheric emission by water bubbles and the attenuation when the wave travels from the ocean surface to the radiometer. $\overline{T}_F$ is the brightness temperature of the foam layer with the consideration of scattering of atmospheric emission and attenuation. T_A is the brightness temperature due to the thermal emission of the atmosphere.

4.3. Equivalent Polar Angle of the Spherical Atmospheric Layer

Consider a radiometer placed at point A with zenith height H as shown in Fig. 8. We create a flat atmospheric layer to approximate the spherical layer so that it is easier to apply the geometry for the RT theory. On the flat layer, the equivalent position of the radiometer is at point C, where we assume $\overline{AB} = \overline{BC}$. It can be found that in the equivalent flat-layer model of the atmosphere, the polar angle θ' is different from θ in the spherical model. By projecting the lines $\overline{AO}$ and $\overline{AB}$ on the x- and z-axis, respectively, we find

$$\overline{AB} \cdot \sin\theta = (R + H) \sin\theta_o, \tag{95}$$

$$R + \overline{AB} \cdot \cos\theta = (R + H) \cos\theta_o. \tag{96}$$

By eliminating the angle θ_o from Eqs. (95) and (96), it yields

$$\overline{AB} = \sqrt{R^2 \cos^2\theta + 2RH + H^2} - R\cos\theta. \tag{97}$$

Considering the triangle BCD, it can be shown that

$$\cos\theta' = H \Big/ \overline{AB}. \tag{98}$$

Therefore the modified polar angle in the equivalent flat atmospheric layer is

$$\theta' = \cos^{-1} \frac{H}{\sqrt{R^2 \cos^2\theta + 2RH + H^2} - R\cos\theta}. \tag{99}$$

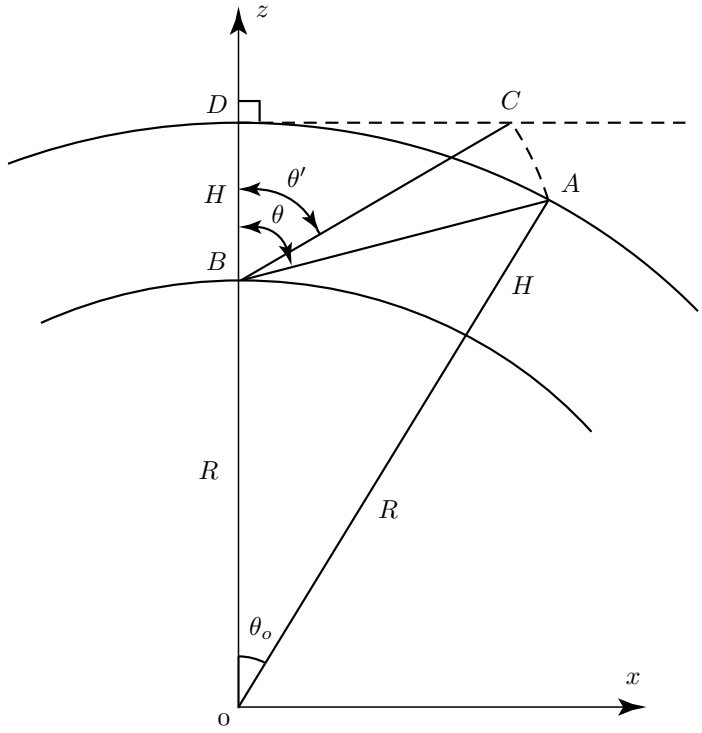

Figure 8. Geometry of the spherical atmospheric layer.

For example, let the radiometer height $H = 30,000$ m, and the earth radius $R = 6.37 \times 10^6$ m. For the zero grazing angle ($\theta = 90°$), the modified polar angle can be calculated as

$$\theta' = \cos^{-1} \frac{H}{\sqrt{2RH + H^2}} = \cos^{-1} \frac{3}{\sqrt{2 \times 637 \times 3 + 3^2}} = 87.2°. \quad (100)$$

5. TWO-SCALE MODEL OF ROUGH OCEAN SURFACE

In the previous section, we only considered the rough ocean surface with wavenumber less than 5 times the electromagnetic wavelength by defining the cutoff wavenumber $k_d = k_o/5$, where k_o is the electromagnetic wavenumber. For numerical purposes, the variable l is defined as $l = 1/k$ so that the integration for l is from 0 to $1/k_d$ instead of from 0 to ∞ for k. Therefore numerically k_d cannot be zero, and the waves are separated into large-scale ($k < k_d$) and small-scale ($k > k_d$) categories. If we only consider the small-scale waves, the total

brightness temperature is not sensitive to the value of k_d (k_d around $k_o/5$) that will be demonstrated in Fig. 14 in the numerical simulation section. The large-scale wave operates as tilted facet. The two-scale model takes care of the tilted polar angle on the local facet due to the large scale or long waves of the ocean surface. In the two-scale model, the brightness temperature vector is calculated by averaging the local values over the slope distribution of the large scale waves [25, 18]. The averaged brightness temperature at the ocean surface is written as

$$\overline{T}(\theta,\phi,0) = \int_{-\infty}^{\infty} dS_x \int_{-\cot\theta}^{\infty} dS_y \overline{T}_l(\theta',\phi) P_s\left(S'_x, S'_y, \theta\right), \tag{101}$$

where $\overline{T}_l(\theta',\phi)$ is the brightness temperature of the local facet at the local looking angle θ', P_s is the slope distribution of the large-scale waves as viewed at the local looking angle θ', S_x and S_y are the surface slopes along the global x and y axis, respectively, while S'_x and S'_y are the surface slopes with respect to the radiometer observation direction (θ',ϕ). Notice that S_x is limited to $-\cot\theta$ due to shadowing by large-scale waves [18]. The transformation of the global slopes to the slopes with respect to the radiometer observation direction is given by

$$S'_x = S_x\cos\phi + S_y\sin\phi, \tag{102}$$

$$S'_y = -S_x\sin\phi + S_y\cos\phi. \tag{103}$$

To calculate the polar angle θ' with respect to the local facet Π for a given looking angle θ with respect to the global coordinate (x,y,z) as shown in Fig. 9, we write the unit normal vector of the local facet as

$$\hat{n} = \frac{\hat{z} - S_x\hat{x} - S_y\hat{y}}{\sqrt{1+S_x^2+S_y^2}}, \tag{104}$$

and the unit wave vector with the orientation angles θ and ϕ as

$$\hat{k} = \hat{x}\sin\theta\cos\phi + \hat{y}\sin\theta\sin\phi + \hat{z}\cos\theta. \tag{105}$$

Thus the polar angle with respect to the local facet is

$$\theta' = \cos^{-1}\hat{k}\cdot\hat{n} = \cos^{-1}\frac{-S_x\sin\theta\cos\phi - S_y\sin\theta\sin\phi + \cos\theta}{\sqrt{1+S_x^2+S_y^2}}. \tag{106}$$

The slope distribution P_s was studied by Cox and Munk [26] by measuring the ocean surface, and it can be written as

$$P_s\left(S'_x, S'_y, \theta\right) = (1 + S_x\tan\theta)\, P\left(S'_x, S'_y\right), \tag{107}$$

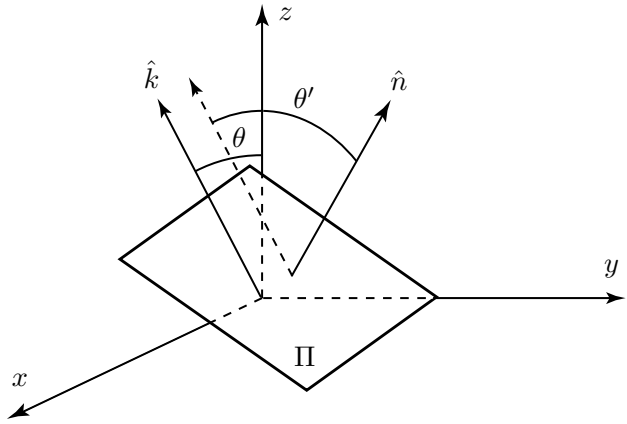

Figure 9. The local polar angle with respect to the global looking angle and the slope of the facet.

where $P(S'_x, S'_y)$ is assumed to be a Gaussian distribution function

$$P\left(S'_x, S'_y\right) = \frac{F\left(S'_x, S'_y\right)}{2\pi S_u S_c} \exp\left[-\left(\frac{{S'_x}^2}{2S_u^2} + \frac{{S'_y}^2}{2S_c^2}\right)\right] \tag{108}$$

with the function $F(S'_x, S'_y)$ defined as

$$\begin{aligned} F\left(S'_x, S'_y\right) \;=\; & 1 - \frac{C_{21}}{2}\left(\frac{{S'_y}^2}{S_c^2} - 1\right)\frac{S'_x}{S_u} - \frac{C_{03}}{6}\left(\frac{{S'_x}^3}{S_u^3} - 3\frac{S'_x}{S_u}\right) \\ & + \frac{C_{40}}{24}\left(\frac{{S'_y}^4}{S_c^4} - 6\frac{{S'_y}^3}{S_c^3} + 3\right) \\ & + \frac{C_{22}}{4}\left(\frac{{S'_y}^2}{S_c^2} - 1\right)\left(\frac{{S'_x}^2}{S_u^2} - 1\right) \\ & + \frac{C_{04}}{24}\left(\frac{{S'_x}^4}{S_u^4} - 6\frac{{S'}^3_u}{S_u^3} + 3\right). \end{aligned} \tag{109}$$

In the above expression, the coefficients are $C_{40} = 0.4$, $C_{22} = 0.12$, $C_{04} = 0.23$, $C_{21} = 0.01 - 0.0086U_w$, and $C_{03} = 0.04 - 0.033U_w$, where U_w is the wind speed in m/s.

The upwind and crosswind slope variances are calculated as

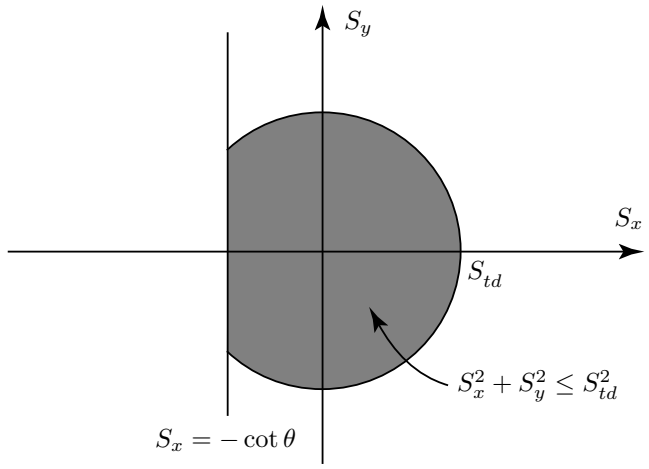

Figure 10. The integration area for determining the slope threshold.

follows:

$$S_u^2 = \int_0^{k_d} dk \int_0^{2\pi} d\phi k^3 \cos^2\phi W(k,\phi), \tag{110}$$

$$S_c^2 = \int_0^{k_d} dk \int_0^{2\pi} d\phi k^3 \sin^2\phi W(k,\phi). \tag{111}$$

In the numerical evaluation of Eq. (101), the integration limits of S_x and S_y are truncated as $5S_u$ and $5S_c$, respectively. The local brightness temperature $\overline{T}_l$ is assigned to be the one of the plain ocean surface $\overline{T}_u^{AS}$ as in Eq. (60) or of the foam $\overline{T}_u^F$ as in Eq. (30) based on the slope of the surface $S = \sqrt{S_x^2 + S_y^2}$. To the best of our knowledge, there is presently no literature on the study of the foam assignment according to the slope of the ocean surface. In this thesis, we assume a threshold S_{td} and assign the foam brightness temperature $\overline{T}_u^F$ to the local $\overline{T}_l$ if the slope $\sqrt{S_x^2 + S_y^2} \geq S_{td}$. The slope threshold S_{td} can be found by calculating the integral within the area [as shown in Fig. 10] of $\left\{(S_x, S_y) : S_x^2 + S_y^2 \leq S_{td}^2, S_x \geq -\cot\theta\right\}$, so that the integral value is equal to the foam coverage F in Eq. (33), i.e.,

$$F = \int dS_y \int dS_x P_s(S'_x, S'_x). \tag{112}$$

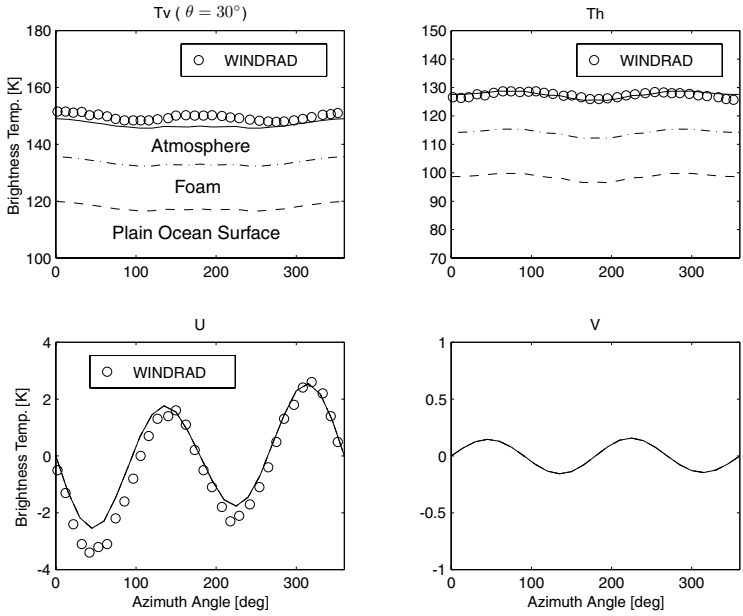

Figure 11. The brightness temperature of wind-driven ocean surface for nadir looking angle $\theta = 30^\circ$ and the lower cutoff wavenumber $k_d = 80$ m^{-1}.

6. NUMERICAL RESULTS

In this section, we calculate the brightness temperature of the wind-driven ocean surface and compare the simulation results with the data from JPL's WINDRAD experiment [14]. In the experiment, a K-band (19.35 GHz) radiometer was mounted on the NASA DC-8 aircraft flying in a circle at the height of 30,000 ft (9,144 m). The data was collected in November 1993 near the northern Californian coast. During the experiment, weather was clear and there was a wind speed of 12 m/s. The brightness temperatures were measured for the Stokes parameters T_v, T_h, and U with the polar angles of 30, 40, and 50 degrees. In the simulation, the frequency of the brightness temperatures is $f = 19.35$ MHz, the ocean wind speed is $U_w = 12$ m/s at height $h = 19.5$ m. The physical temperature of the sea water is $T_o = 12$ °C, and the salinity is $S = 3.5\%$.

Figs. 11, 12 and 13 show the simulation results of the brightness temperatures by varying the azimuth angle ϕ of the observation with nadir looking angle $\theta = 30^\circ$, 40° and 50°, respectively. The ocean surface spectrum is the empirical formula proposed by Durden and

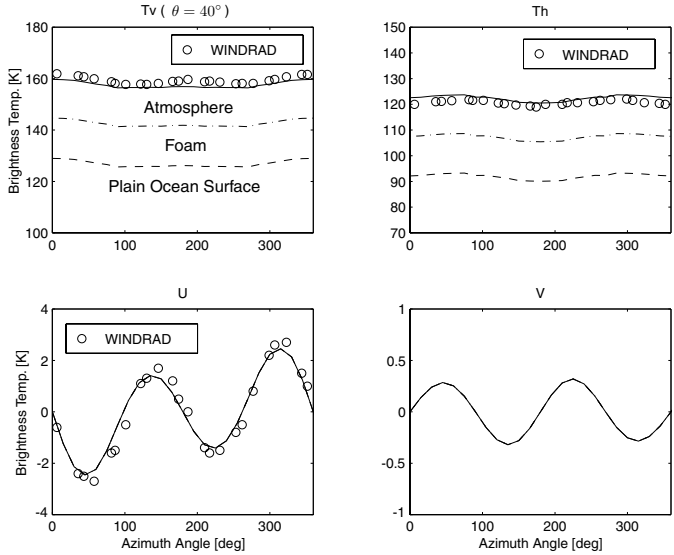

Figure 12. The brightness temperature of wind-driven ocean surface for nadir looking angle $\theta = 40^\circ$ and the lower cutoff wavenumber $k_d = 80$ m^{-1}.

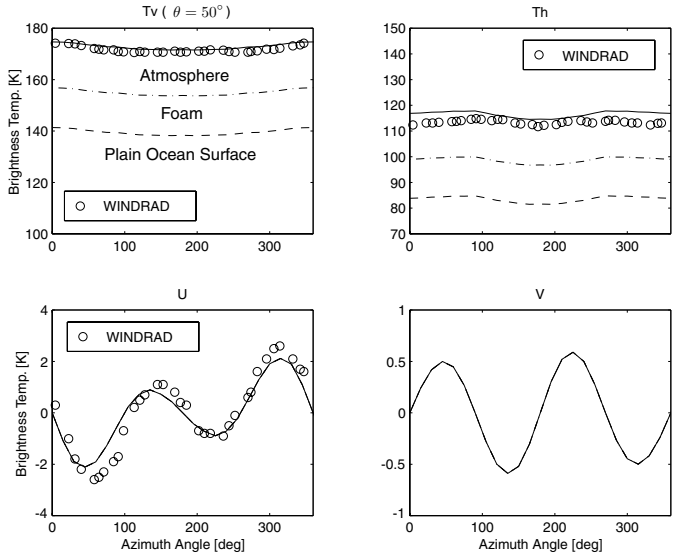

Figure 13. The brightness temperature of wind-driven ocean surface for nadir looking angle $\theta = 50^\circ$ and the lower cutoff wavenumber $k_d = 80$ m^{-1}.

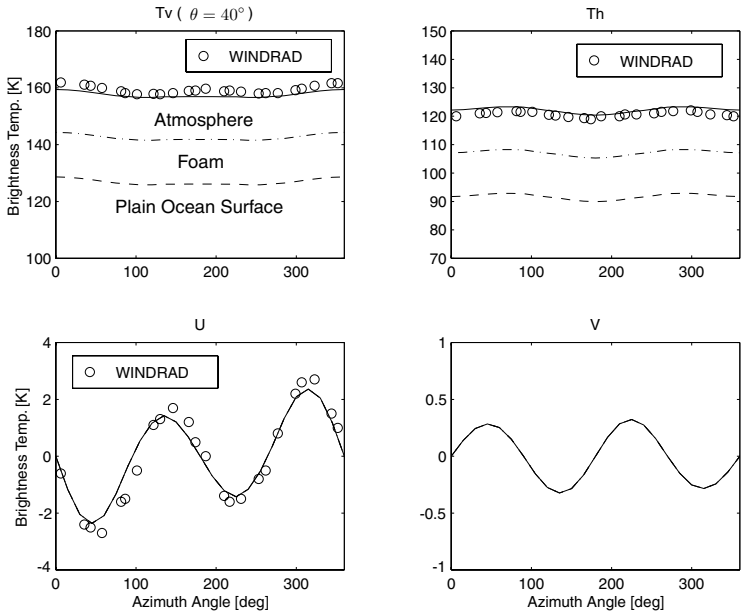

Figure 14. The brightness temperature of wind-driven ocean surface for nadir looking angle $\theta = 40^\circ$ and the lower cutoff wavenumber $k_d = 120$ m^{-1}.

Vesecky [17]. For the foam layer, the internal radius of water bubble is $R = 4.3$ mm, the bubble film thickness is $d = 0.13$ mm and the fractional volume of water bubbles is $f_v = 0.01$. The extinction and absorption coefficients are calculated as $\kappa_e = 8.298$ m^{-1} and $\kappa_a = 2.273$ m^{-1}. The permittivity of the bubble film is the same as of the ocean water, and the permittivity of the background is ϵ_o. The elevation height of the radiometer is 30,000 ft (9,144 m). In these figures, the open circles are the WINDRAD experimental data. In the plots of the first and second Stokes parameters T_v and T_h, the lines (from bottom to top) are the plots for the numerical simulation considering (1) only the plain ocean surface [$\overline{T}_S$ in Eq. (92)], (2) plain ocean surface plus the foam emission [$\overline{T}_S + \overline{T}_F$ in Eq. (92) and (93)], and (3) plain ocean surface plus the foam and the atmospheric emissions [$\overline{T}_S + \overline{T}_F + \overline{T}_A$ in Eq. (92), (93) and (94)]. In the plots for the third and fourth Stokes parameters U and V, the total emissions are considered. In comparison with experiment data, we notice that both the foam and the atmospheric emission are significant to correct the emission of the plain ocean surface for T_v and T_h.

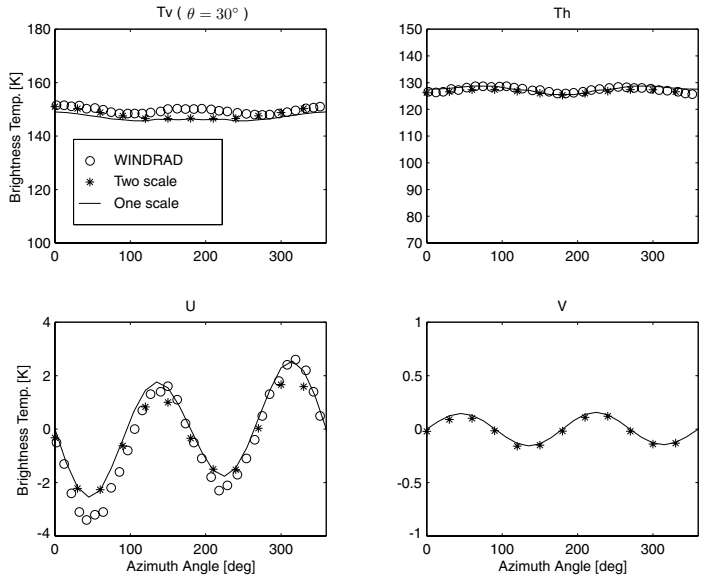

Figure 15. The comparison of the one-scale and two-scale models at $\theta = 30°$.

The Durden-Vesecky spectrum is similar to the power law $W(k) = a_0/k^4$ that describes the relative portion of the large scale and small scale roughness of the ocean surface by specifying the lower cutoff wavenumber k_d. The smaller k_d is, the higher the long waves. However, in the simulation for the thermal emission from the ocean surface, the brightness temperatures are obtained by integrating over the entire reflected waves due to Kirchhoff's law. Therefore there is no significant difference between the collection of reflected waves from very long ocean waves or from a flat surface. In SPM, the zeroth and the second order reflected waves are specular, thus they include the dominant reflections from the long waves. The bistatic pattern of the field scattered by rough ocean surface is dominated by small scale roughness (Bragg scattering) which is included in the first order solution in SPM. Therefore the value of the lower cutoff wavenumber k_d is not sensitive to the calculation of the emissivity from the rough ocean surface. This can be demonstrated by re-calculating the brightness temperatures shown in Figs. 11, 12 and 13 with lower cutoff wavenumbers. In Figs. 11, 12 and 13, the lower cutoff wavenumber is $k_d = 80$ m^{-1} which is about 5λ of the electromagnetic wave. Fig. 14 shows the brightness temperatures for the polar angle $\theta = 40°$ and the lower cutoff wavenumber $k_d = 120$ m^{-1}. Not much change is observed for

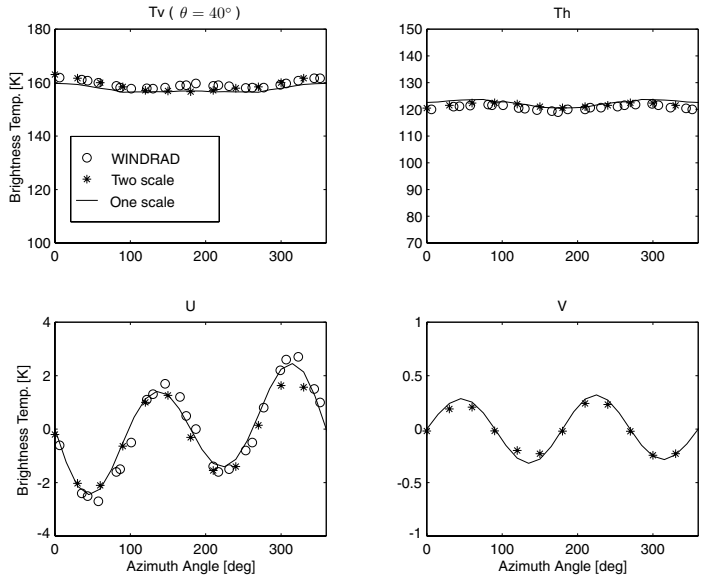

Figure 16. The comparison of the one-scale and two-scale models at $\theta = 40°$.

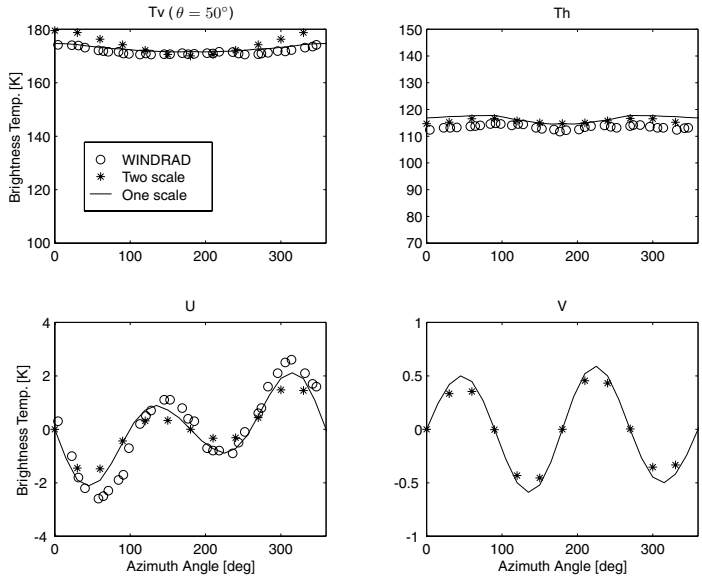

Figure 17. The comparison of the one-scale and two-scale models at $\theta = 50°$.

the result in comparison with Fig. 12 for $k_d = 80$ m^{-1}.

With the same simulation conditions as in Figs. 11–13, we compare the numerical results obtained by using the one-scale and two-scale models as shown in Figs. 15–17. Notice that the T_v and T_h terms in these figures match better with the measurement data in the two-scale model for $\theta = 30^\circ$ and 40°, but there is an irregular offset in Fig. 17, which may be due to the shadowing effect at large polar angles.

7. CONCLUSIONS

In this paper, one-scale and two-scale electromagnetic models to calculate the brightness temperature of wind-driven ocean with foam coverage have been presented. The one-scale emissivity model is the local thermal contribution by small roughness of the foam-covered ocean surface, while the two-scale model is the average of one-scale emissivity over large-scale slope of the rough ocean surface with the weight described by the slope distribution function. The overall brightness temperature is contributed by three portions — plain ocean surface, foam, and atmospheric layer. The interactions between the different regions are described by boundary conditions. For the plain ocean surface, the emissivity has been calculated using Kirchhoff's law by calculating the reflectivity of rough ocean surface. The coupling to the wind speed is through the power spectrum of ocean surface by which the ocean rough surface is described. The radiative transfer theory (RT) is used to model the foam layer in which we assume the scatterers are spherical thin-film water bubbles. The closed form solution of the RT equations for the foam layer is obtained using the iterative approach up to the first order. In the RT equations for the atmospheric layer, the scattering due to the water vapor and other gases in the air is ignored, hence a closed form of the RT solution is obtained. The simulation results, both from one-scale and two-scale models, are compared with the WINDRAD experimental data with good agreements. The results show that both the one-scale and two-scale models agree well with the WINDRAD data. However the one-scale model is much faster in computation than the two-scale model, since few integrals are involved in the one-scale model.

It has to be pointed out that, although the foam model with water bubbles is more realistic than water particles, more studies need to be conducted to model the foam layer more accurately. For example, it is suggested the multiple scattering among water bubbles to be considered by using the dense medium radiative transfer theory [15], and the top foam surface to be rough instead of flat as considered in this paper for simplification.

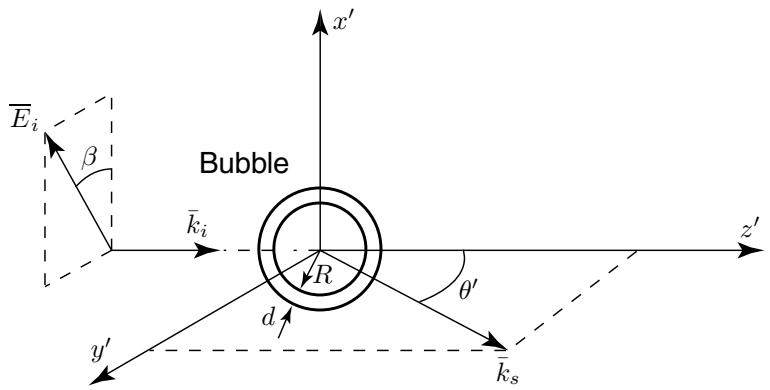

Figure A1. EM scattering by a bubble in (x', y', z') coordinates.

APPENDIX A. PHASE MATRIX FOR WATER BUBBLES

Consider an electromagnetic plane wave propagating in $+\hat{z}'$ direction and incident upon a thin-film water bubble in (x', y', z') coordinates with inner radius R and film thickness d as shown in Fig. A1. Let the wavenumber in the core and outside be k, the wavenumber in the film be k_1, and the polarization angle be β.

On $y'z'$ plane, the scattered field with scattering angles θ' and $\phi' = 90^\circ$ in radiation zone is given in a closed form as follows [27]:

$$E_{\phi'} = \frac{ie^{ikr}}{kr} S_1 \cos\beta, \tag{A1}$$

$$E_{\theta'} = -\frac{ie^{ikr}}{kr} S_2 \sin\beta, \tag{A2}$$

where

$$S_1 = i\delta(m^2-1)\alpha^2 \left[j_o(x) - \frac{m^2-1}{m^2} \frac{j_1(x)}{x} \right], \tag{A3}$$

$$S_2 = i\delta(m^2-1)\alpha^2 \Bigg\{ j_o(x)\cos\theta' + \frac{m^2-1}{m^2} \left[\frac{j_1(x)}{x} + \frac{1+\cos\theta'}{2} \left(\frac{j_1(x)}{x} - j_o(x) \right) \right] \Bigg\}, \tag{A4}$$

in which $m = k_1/k$, $x = \dfrac{4\pi}{\lambda} R \sin(\theta'/2)$, $\delta = 2\pi d/\lambda$, $\alpha = 2\pi R/\lambda$, $j_o(x)$ and $j_1(x)$ are the zeroth and first order spherical Bessel's functions,

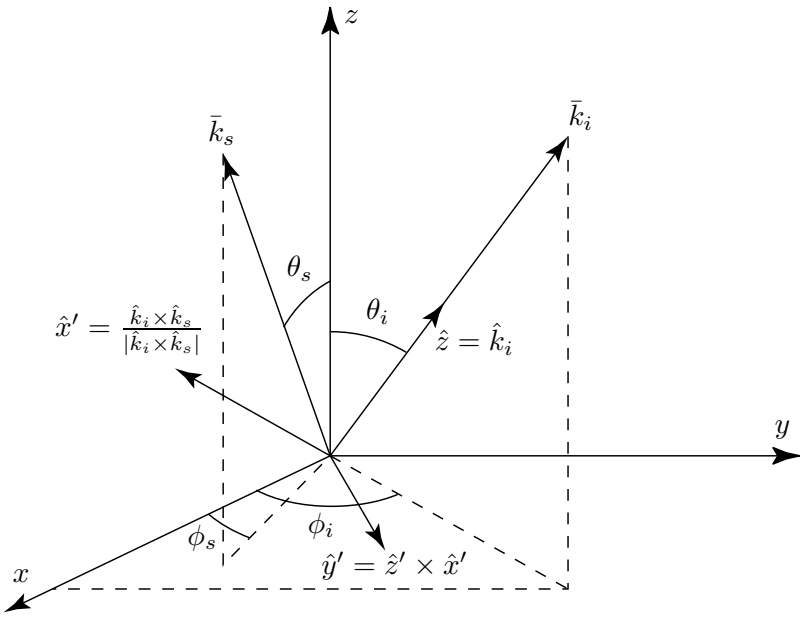

Figure A2. The transformation of coordinates.

respectively. The geometry of the wave scattering in (x', y', z') coordinates is general because of the symmetrical property of the spherical water bubble.

In the (x, y, z) coordinate system, the incident wave is written as

$$\overline{E}_i = \hat{e}_i E_o e^{i\bar{k}_i \cdot \bar{r}}, \tag{A5}$$

where $\hat{e}_i = \hat{v}_i$ or $\hat{h}_i$, $E_{e_i} = E_{v_i}$ or E_{h_i}, and

$$\bar{k}_i = k\hat{k}_i = k(\hat{x}\sin\theta_i\cos\phi_i + \hat{y}\sin\theta_i\sin\phi_i + \hat{z}\cos\theta_i),$$

and the incident angles θ_i and ϕ_i are with respect to the (x, y, z) coordinates as shown in Fig. A2. The polarization vectors are defined as

$$\begin{cases} \hat{v}_i = \hat{h}_i \times \hat{k}_i = \hat{x}\cos\theta_i\cos\phi_i + \hat{y}\cos\theta_i\sin\phi_i - \hat{z}\sin\theta_i, \\ \hat{h}_i = \dfrac{\hat{z} \times \hat{k}_i}{\left|\hat{z} \times \hat{k}_i\right|} = -\hat{x}\sin\phi_i + \hat{y}\cos\phi_i. \end{cases} \tag{A6}$$

In the (x, y, z) coordinate system, we set up the coordinates (x', y', z')

so that

$$\begin{cases} \hat{x}' = \dfrac{\hat{k}_i \times \hat{k}_s}{\left|\hat{k}_i \times \hat{k}_s\right|}, \\ \hat{y}' = \dfrac{\hat{k}_i \times \hat{k}_i \times \hat{k}_s}{\left|\hat{k}_i \times \hat{k}_i \times \hat{k}_s\right|} = \dfrac{\hat{k}_i\left(\hat{k}_i \cdot \hat{k}_s\right) - \hat{k}_s}{\left|\hat{k}_i\left(\hat{k}_i \cdot \hat{k}_s\right) - \hat{k}_s\right|}, \\ \hat{z}' = \hat{k}_i, \end{cases} \tag{A7}$$

where

$$\hat{k}_s = \hat{x}\sin\theta_s\cos\phi_s + \hat{y}\sin\theta_s\sin\phi_s + \hat{z}\cos\theta_s$$

is the wave vector of the scattered field. Therefore the transformation relation of the two coordinate systems is

$$\begin{cases} \hat{x}' = \hat{x}a_{11} + \hat{y}a_{12} + \hat{z}a_{13} \\ \hat{y}' = \hat{x}a_{21} + \hat{y}a_{22} + \hat{z}a_{23} \\ \hat{z}' = \hat{x}a_{31} + \hat{y}a_{32} + \hat{z}a_{33} \end{cases} \tag{A8}$$

or

$$\begin{bmatrix} \hat{x}' \\ \hat{y}' \\ \hat{z}' \end{bmatrix} = \overline{\overline{A}} \begin{bmatrix} \hat{x} \\ \hat{y} \\ \hat{z} \end{bmatrix} \tag{A9}$$

where

$$\begin{cases} a_{11} = \begin{vmatrix} a_{22} & a_{23} \\ a_{32} & a_{33} \end{vmatrix} \\ a_{12} = \begin{vmatrix} a_{31} & a_{33} \\ a_{21} & a_{23} \end{vmatrix} \\ a_{13} = \begin{vmatrix} a_{21} & a_{31} \\ a_{22} & a_{32} \end{vmatrix} \end{cases} \tag{A10}$$

$$\begin{cases} a_{21} = \dfrac{A_{21}}{\sqrt{A_{21}^2 + A_{22}^2 + A_{23}^2}} \\ a_{22} = \dfrac{A_{22}}{\sqrt{A_{21}^2 + A_{22}^2 + A_{23}^2}} \\ a_{23} = \dfrac{A_{23}}{\sqrt{A_{21}^2 + A_{22}^2 + A_{23}^2}} \end{cases} \tag{A11}$$

$$\begin{cases} a_{31} = \sin\theta_i \cos\phi_i \\ a_{32} = \sin\theta_i \sin\phi_i \\ a_{33} = \cos\theta_i \end{cases} \tag{A12}$$

$$\begin{cases} A = \sin\theta_i \sin\theta_s \cos(\phi_i - \phi_s) + \cos\theta_i \cos\theta_s \\ A_{21} = A\sin\theta_i \cos\phi_i - \sin\theta_s \cos\phi_s \\ A_{22} = A\sin\theta_i \sin\phi_i - \sin\theta_s \sin\phi_s \\ A_{23} = A\cos\theta_i - \cos\theta_s \end{cases} \tag{A13}$$

By using the identity $\overline{\overline{A}}^{-1} = \overline{\overline{A}}^{T}$, the transformation of a vector from one coordinate system to another can the expressed as

$$\overline{E}' = E'^{T} \begin{bmatrix} \hat{x}' \\ \hat{y}' \\ \hat{z}' \end{bmatrix} = E'^{T} \overline{\overline{A}} \begin{bmatrix} \hat{x} \\ \hat{y} \\ \hat{z} \end{bmatrix} \equiv \overline{E}. \tag{A14}$$

Thus $E = \overline{\overline{A}}^{T} E'$ and $E' = \overline{\overline{A}} E$.

By writing the incident field in (x, y, z) coordinates as

$$\overline{E}_i = \hat{e}_i E_o e^{i\bar{k}_i \cdot \bar{r}} = E_o[(\hat{e}_i \cdot \hat{x})\hat{x} + (\hat{e}_i \cdot \hat{y})\hat{y} + (\hat{e}_i \cdot \hat{z})\hat{z}]e^{i\bar{k}_i \cdot \bar{r}}, \tag{A15}$$

thus the transformation of the incident field is

$$\overline{E}_i' = \begin{bmatrix} E_{x'}^i \\ E_{y'}^i \\ E_{z'}^i \end{bmatrix} = \overline{\overline{A}} \begin{bmatrix} (\hat{e}_i \cdot \hat{x}) \\ (\hat{e}_i \cdot \hat{y}) \\ (\hat{e}_i \cdot \hat{z}) \end{bmatrix} E_o = \begin{bmatrix} a_{11} & a_{12} & a_{13} \\ a_{21} & a_{22} & a_{23} \\ a_{31} & a_{32} & a_{33} \end{bmatrix} \begin{bmatrix} (\hat{e}_i \cdot \hat{x}) \\ (\hat{e}_i \cdot \hat{y}) \\ (\hat{e}_i \cdot \hat{z}) \end{bmatrix} E_o, \tag{A16}$$

we can calculate the polarization angle β and scattering angle θ' in the (x', y', z') coordinates as follows:

$$\beta = \cos^{-1} \frac{\overline{E}_i' \cdot \hat{y}'}{\left|\overline{E}_i'\right|} = \cos^{-1} \frac{b_2}{C}, \tag{A17}$$

$$\theta' = \cos^{-1} \hat{k}_s \cdot \hat{z}' = \cos^{-1}[\sin\theta_i \sin\theta_s \cos(\phi_s - \phi_i) + \cos\theta_i \cos\theta_s], \tag{A18}$$

where

$$b_1 = a_{11}(\hat{e}_i \cdot \hat{x}) + a_{12}(\hat{e}_i \cdot \hat{y}) + a_{13}(\hat{e}_i \cdot \hat{z}), \tag{A19}$$

$$b_2 = a_{21}(\hat{e}_i \cdot \hat{x}) + a_{22}(\hat{e}_i \cdot \hat{y}) + a_{23}(\hat{e}_i \cdot \hat{z}), \tag{A20}$$

$$b_3 = a_{31}(\hat{e}_i \cdot \hat{x}) + a_{32}(\hat{e}_i \cdot \hat{y}) + a_{33}(\hat{e}_i \cdot \hat{z}), \tag{A21}$$

$$C = \sqrt{b_1^2 + b_2^2 + b_3^2}. \tag{A22}$$

In the (x', y', z') coordinate system, we write the scattered field as

$$\overline{E}_s' = E_{\theta'}\hat{\theta}' + E_{\phi'}\hat{\phi}' = E_{\theta'}(\hat{y}' \cos\theta' - \hat{z}' \sin\theta') - E_{\phi'}\hat{x}'$$
$$= \begin{bmatrix} -E_{\phi'} \\ E_{\theta'} \cos\theta' \\ -E_{\theta'} \sin\theta' \end{bmatrix}, \tag{A23}$$

where, by dropping out the factor $\dfrac{e^{ikr}}{r}$ for scattering coefficient calculation,

$$E_{\phi'} = \frac{i}{k} S_1 \cos\beta, \tag{A24}$$

$$E_{\theta'} = -\frac{i}{k} S_2 \sin\beta. \tag{A25}$$

The scattered field in the (x, y, z) coordinate system is thus

$$\begin{aligned}\overline{E}_s &= \overline{\overline{A}}^T \overline{E}'_s = \begin{bmatrix} a_{11} & a_{21} & a_{31} \\ a_{12} & a_{22} & a_{32} \\ a_{13} & a_{23} & a_{33} \end{bmatrix} \begin{bmatrix} -E_{\phi'} \\ E_{\theta'} \cos\theta' \\ -E_{\theta'} \sin\theta' \end{bmatrix} \\ &= \begin{bmatrix} -E_{\phi'} a_{11} + E_{\theta'} \cos\theta' a_{21} - E_{\theta'} \sin\theta' a_{31} \\ -E_{\phi'} a_{12} + E_{\theta'} \cos\theta' a_{22} - E_{\theta'} \sin\theta' a_{32} \\ -E_{\phi'} a_{13} + E_{\theta'} \cos\theta' a_{23} - E_{\theta'} \sin\theta' a_{33} \end{bmatrix}. \end{aligned} \tag{A26}$$

By writing the polarization vectors of the scattered field as

$$\begin{cases} \hat{v}_s = \hat{h}_s \times \hat{k}_s = \hat{x} \cos\theta_s \cos\phi_s + \hat{y} \cos\theta_s \sin\phi_s - \hat{z} \sin\theta_s, \\ \hat{h}_s = \dfrac{\hat{z} \times \hat{k}_s}{\left| \hat{z} \times \hat{k}_s \right|} = -\hat{x} \sin\phi_s + \hat{y} \cos\phi_s, \end{cases} \tag{A27}$$

the v and h-components are obtained as follows:

$$\begin{aligned} E_v^s &= \overline{E}_s \cdot \hat{v}_s = \left(-E_{\phi'} a_{11} + E_{\theta'} \cos\theta' a_{21} - E_{\theta'} \sin\theta' a_{31}\right) \cos\theta_s \cos\phi_s \\ &\quad + \left(-E_{\phi'} a_{12} + E_{\theta'} \cos\theta' a_{22} - E_{\theta'} \sin\theta' a_{32}\right) \cos\theta_s \sin\phi_s \\ &\quad + \left(E_{\phi'} a_{13} - E_{\theta'} \cos\theta' a_{23} + E_{\theta'} \sin\theta' a_{33}\right) \sin\theta_s, \end{aligned} \tag{A28}$$

$$\begin{aligned} E_h^s &= \overline{E}_s \cdot \hat{h}_s = \left(E_{\phi'} a_{11} - E_{\theta'} \cos\theta' a_{21} + E_{\theta'} \sin\theta' a_{31}\right) \sin\phi_s \\ &\quad - \left(E_{\phi'} a_{12} - E_{\theta'} \cos\theta' a_{22} + E_{\theta'} \sin\theta' a_{32}\right) \cos\phi_s. \end{aligned} \tag{A29}$$

Therefore the scattering coefficients are $f_{vv} = E_v^s,\ f_{hv} = E_h^s$ for $\hat{e}_i = \hat{v}_i$ and $E_o = 1$; $f_{vh} = E_v^s,\ f_{hh} = E_h^s$ for $\hat{e}_i = \hat{h}_i$ and $E_o = 1$. Define the matrix

$$\overline{\overline{L}}(\theta_s, \phi_s; \theta_i, \phi_i) = \begin{bmatrix} |f_{vv}|^2 & |f_{vh}|^2 & \mathrm{Re}(f_{vv} f_{vh}^*) & -\mathrm{Im}(f_{vv} f_{vh}^*) \\ |f_{hv}|^2 & |f_{hh}|^2 & \mathrm{Re}(f_{hv} f_{hh}^*) & -\mathrm{Im}(f_{hv} f_{hh}^*) \\ 2\mathrm{Re}(f_{vv} f_{hv}^*) & 2\mathrm{Re}(f_{vh} f_{hh}^*) & \mathrm{Re}(f_{vv} f_{hh}^* + f_{vh} f_{hv}^*) & -\mathrm{Im}(f_{vv} f_{hh}^* - f_{vh} f_{hv}^*) \\ 2\mathrm{Im}(f_{vv} f_{hv}^*) & 2\mathrm{Im}(f_{vh} f_{hh}^*) & \mathrm{Im}(f_{vv} f_{hh}^* + f_{vh} f_{hv}^*) & \mathrm{Re}(f_{vv} f_{hh}^* - f_{vh} f_{hv}^*) \end{bmatrix}, \tag{A30}$$

the phase matrix can be calculated as

$$\overline{\overline{P}}(\theta_s, \phi_s; \theta_i, \phi_i) = n_o \overline{\overline{L}}(\theta_s, \phi_s; \theta_i, \phi_i), \tag{A31}$$

where n_o is the number of bubbles per unit volume.

The extinction coefficient is derived as following [15, page 147]:

$$\begin{aligned}\kappa_e &= n_o \frac{4\pi}{k} \mathrm{Im}\{f_{vv}(\theta_i, \phi_i; \theta_i, \phi_i)\} = -n_o \frac{4\pi}{k^2} \mathrm{Im}\{iS_1\} \\ &= n_o \frac{4\pi}{k^2} \mathrm{Im}\left\{\delta(m^2-1)\alpha^2 \left[j_o(x) - \frac{m^2-1}{m^2}\frac{j_1(x)}{x}\right]_{x\to 0}\right\} \\ &= n_o \frac{4\pi}{k^2} \delta\alpha^2 \mathrm{Im}\left\{(m^2-1)\left(\frac{2m^2+1}{3m^2}\right)\right\}. \end{aligned} \tag{A32}$$

The absorption coefficient is

$$\kappa_s = n_o \int d\Omega_s \left[|f_{vv}(\theta_s, \phi_s; \theta_i, \phi_i)|^2 + |f_{hv}(\theta_s, \phi_s; \theta_i, \phi_i)|^2\right], \tag{A33}$$

which can be evaluated numerically. Due to the symmetry property of the bubble, κ_s is independent on the angles θ_i and ϕ_i. The absorption coefficient is calculated as

$$\kappa_a = \kappa_e - \kappa_s. \tag{A34}$$

APPENDIX B. PARAMETERS IN THE MILLIMETER-WAVE PROPAGATION MODEL

The parameters used in the MPM [24] are as follows:

Barometric pressure

$$P = p + e, \tag{B1}$$

where p is dry air pressure and e is partial water vapor pressure. The unit of the barometric pressure is kPa.

Temperature

$$T = 300/t, \tag{B2}$$

where the unit of the temperature is Kelvin (K), and t is the inverse temperature parameter. The typical temperature profile is given in [23] and plotted in Fig. 4.

Relative humidity

$$RH = \frac{e}{e_s} \times 100 = 41.51 \frac{e}{t^5} \times 10^{\frac{9.834}{t^{10}}}, \tag{B3}$$

where e_s is the saturation pressure over liquid phase.

Dry air and vapor densities

$$\begin{aligned} u &= 11.612pt, \\ v &= 7.217et, \end{aligned} \tag{B4}$$

where the unit of the densities is $\mathrm{g/m^3}$.

Complex refractivity

$$N = N_0 + N'(f) + iN''(f), \tag{B5}$$

where N_0, $N'(f)$ and $N''(f)$ are real and called the frequency-independent term, refractive dispersion and absorption, respectively. f is frequency in gigahertz (GHz).

Frequency-independent term

$$N_0 = (2.588p + 2.39e)t + N_v, \tag{B6}$$

where $N_v = 41.6et^2$ is the contribution from the rotational spectrum of water vapor.

Dispersion term

$$N'(f) = \sum_{i=1}^{n_a}(S_a F'_a)_i + N'_p + \sum_{i=1}^{n_b}(S_b F'_b)_i + N'_e + N'_w, \tag{B7}$$

Absorption term

$$N''(f) = \sum_{i=1}^{n_a}(S_a F''_a)_i + N''_p + \sum_{i=1}^{n_b}(S_b F''_b)_i + N''_e + N''_w, \tag{B8}$$

where $S_a = a_1 pt^3 e^{a_2(1-t)}$ and $S_b = b_1 et^{3.5} e^{b_2(1-t)}$ are the line strength in kilohertz for oxygen and water, respectively. F'_a and F'_b are the real parts of a line shape function in $\mathrm{GHz^{-1}}$ which can be written explicitly as

$$F'_\alpha(f) = \frac{Z_\alpha - f}{X_\alpha} + \frac{Z_\alpha + f}{Y_\alpha} - \frac{2}{\upsilon_{\alpha o}} + \delta_\alpha \left(\frac{1}{X_\alpha} - \frac{1}{Y_\alpha}\right)\frac{\gamma_\alpha f}{\upsilon_{\alpha o}}, \tag{B9}$$

$$F''_\alpha(f) = -\delta_\alpha \left[\frac{\upsilon_{\alpha o} - f}{X_\alpha} + \frac{\upsilon_{\alpha o} + f}{Y_\alpha}\right]\frac{f}{\upsilon_{\alpha o}} + \left(\frac{1}{X_\alpha} + \frac{1}{Y_\alpha}\right)\frac{\gamma_\alpha f}{\upsilon_{\alpha o}}, \tag{B10}$$

where $\alpha = a, b$, and

$$\begin{aligned} X_\alpha &= (\upsilon_{\alpha o} - f)^2 + \gamma_\alpha^2, \\ Y_\alpha &= (\upsilon_{\alpha o} + f)^2 + \gamma_\alpha^2, \\ Z_\alpha &= (\upsilon_{\alpha o}^2 + \gamma_\alpha^2)/\upsilon_{\alpha o}, \\ \gamma_a &= a_3 \left(pt^{0.8-a_4} + 1.1et \right), \\ \gamma_b &= b_3 \left(pt^{0.8} + 4.8et \right), \\ \delta_a &= a_5 pt^{a_6}, \\ \delta_b &= 0. \end{aligned}$$

In the above expressions, υ_{oa} and a_i $(i = 1, 2, \ldots, 6)$ are oxygen line parameters, υ_{ob}, and b_i $(i = 1, 2, 3)$ are water vapor line parameters.

Dry air continuum

$$N_p'(f) = a_0 \left\{ \left[1 + (f/\gamma_0)^2 \right]^{-1} - 1 \right\} pt^2, \tag{B11}$$

$$N_p''(f) = \left\{ 2a_0 \left[\gamma_0 \left(1 + (f/\gamma_0)^2 \right) \left(1 + (f/60)^2 \right) \right]^{-1} + a_p pt^{2.5} \right\} fpt^2, \tag{B12}$$

where $a_0 = 3.07 \times 10^{-4}$, $a_p = 1.40(1 - 1.2f^{1.5}10^{-5})10^{-10}$, and $\gamma_0 = 5.6 \times 10^{-3}(p + 1.1e)t^{0.8}$ GHz.

Water vapor continuum

$$N_e'(f) = b_0 f^{2.05} et^{2.4}, \tag{B13}$$

$$N_e''(f) = \left(b_f p + b_e et^3 \right) fet^{2.5}, \tag{B14}$$

where $b_0 = 6.47 \times 10^{-6}$, $b_f = 1.40 \times 10^{-6}$ and $b_e = 5.41 \times 10^{-5}$.

Hydrosol continuum

$$N_w'(f) = 2.4 \times 10^{-3} w\epsilon', \tag{B15}$$

$$N_w''(f) = 4.50 w/\epsilon''(1 + \eta^2), \tag{B16}$$

where $\eta = (2 + \epsilon')/\epsilon''$ and $\tau = 4.17 \times 10^{-5} te^{(7.13t)}$ ns. ϵ' and ϵ'' are the real and imaginary parts of the dielectric constant of water. They can be calculated using the following empirical formulas

$$\epsilon' = 4.9 + \frac{185 - 113/t}{1 + (f\tau)^2}, \tag{B17}$$

$$\epsilon'' = \frac{(185 - 113/t) f\tau}{1 + (f\tau)^2}. \tag{B18}$$

REFERENCES

1. Yueh, S. H., R. Kwok, F. K. Li, S. V. Nghiem, and W. J. Wilson, "Polarimetric passive remote sensing of ocean wind vectors," *Radio Sci.*, Vol. 29, No. 4, 799–814, July–Aug. 1994.
2. Yueh, S. H., S. V. Nghiem, R. Kwok, W. J. Wilson, F. K. Li, J. T. Johnson, and J. A. Kong, "Polarimetric thermal emission from periodic water surface," *Radio Sci.*, Vol. 29, No. 1, 87–96, Jan.–Feb. 1994.
3. Johnson, J. T., J. A. Kong, R. T. Shin, D. H. Staelin, K. O'Neill, and A. W. Lananick, "Third Stokes parameter emission from a periodic water surface," *IEEE Trans. Geosci. Remote Sensing*, Vol. 31, No. 5, 1066–1080, Sept. 1993.
4. Johnson, J. T., J. A. Kong, R. T. Shin, S. H. Yueh, S. V. Nghiem, and R. Kwok, "Polarimetric thermal emission from rough ocean surfaces," *J. Electromagnetic Waves and Applications*, Vol. 8, No. 1, 43–59, 1994.
5. Williams, G. F., "Microwave radiometry of the ocean and the possibility of marine wind velocity determination from satellite observations," *J. Geophys. Res.*, Vol. 74, No. 18, 4591–4594, Aug. 1969.
6. Williams, G. F., "Microwave emissivity measurements of bubbles and foam," *IEEE Trans. Geosci. Electron.*, GE-9, No. 4, 221–224, Oct. 1971.
7. Smith, P. M., "The emissivity of sea foam at 19 and 37 GHz," *IEEE Trans. Geosci. Remote Sensing*, Vol. 26, No. 5, 541–547, Sept. 1988.
8. Stogryn, A., "The emissivity of sea foam at microwave frequencies," *J. Geophys. Res.*, Vol. 77, No. 9, 1658–1666, Mar. 1972.
9. Pandey, P. C. and R. K. Kakar, "An empirical microwave emissivity model for a foam-covered sea," *IEEE J. Oceanic Eng.*, OE-7, No. 3, 135–140, July 1982.
10. Droppleman, J. D., "Apparent microwave emissivity of sea foam," *J. Geophys. Res.*, Vol. 75, No. 3, 696–698, Jan. 1970.
11. Rosenkranz, P. W., and D. H. Staelin, "Microwave emissivity of ocean foam and its effect on nadiral radiometric measurements," *J. Geophys. Res.*, Vol. 77, No. 33, 6528–6538, Nov. 1972.
12. Huang, X. Z. and Y. Q. Jin, "Scattering and emission from two-scale randomly rough sea surface with foam scatterers," *IEE Proc. H (Microwaves, Antennas and Propagat.)*, Vol. 142, No. 2, 109–114, Apr. 1995.

13. Manahan, E. C. and G. MacNiocaill, *Oceanic Whitecaps and Their Role in Air-Sea Exchange Processes*, D. Reidel Pub. Co., Boston, 1986.
14. Yueh, S. H., W. J. Wilson, F. K. Li, S. V. Nghiem, and W. B. Ricketts, "Polarimetric measurements of sea surface brightness temperatures using an aircraft K-band radiometer," *IEEE Trans. Geosci. Remote Sensing.*, Vol. 33, No. 1, 85–92, Jan. 1995.
15. Tsang, L., J. A. Kong, and R. T. Shin, *Theory of Microwave Remote Sensing*, Wiley, New York, 1985.
16. Shin, R. T. and J. A. Kong, "Radiative transfer theory for active remote sensing of two-layer random medium," *Progress in Electromagnetics Research (PIER 1)*, J. A. Kong (Ed.), Elsevier Science, New York, 1989.
17. Durden, S. P. and J. F. Vesecky, "A physical radar cross-section model for a wind-driven sea with swell," *IEEE J. Oceanic Eng.*, OE-10, 445–457, Oct. 1985.
18. Yueh, S. H., "Modeling of wind direction signals in polarimetric sea surface brightness temperature," *IEEE Trans. Geosci. Remote Sensing.*, Vol. 35, No. 6, 1400–1418, Nov. 1997.
19. Liebe, H. J., "MPM—an atmospheric millimeter-wave propagation model," *Int'l J. Infr. Millimeter Waves.*, Vol. 10, No. 6, 631–650, June 1989.
20. Hunt, G. E., "A review of computational techniques for analysing the transfer of radiation through a model cloudy atmosphere," *J. Quant. Spectrosc. Radiat. Transfer.*, Vol. 11, No. 6, 655–690, June 1971.
21. Brussaard, G. and P. A. Watson, *Atmospheric Modeling and Millimeter Wave Propagation*, Chapman & Hall, 1995.
22. Yeang, C. P., S. H. Yueh, K. H. Ding, and J. A. Kong, "Atmospheric effect on microwave polarimetric passive remote sensing of ocean surfaces," *Radio Sci.*, Vol. 34, No. 2, 521–537, Mar.–April 1999.
23. *U.S. Standard Atmosphere*, National Oceanic and Atmospheric Administration, National Aeronautics and Space Administration, United States Air Force, 1976.
24. Liebe, H. J., "An updated model for millimeter wave propagation in moist air," *Radio Sci.*, Vol. 20, No. 5, 1069–1089, Sept.–Oct. 1985.
25. Chan, H. L. and A. K. Fung, "A theory of sea scatter at large incident angles," *J. Geophys. Res.*, Vol. 82, No. 24, 3439–3444,

Aug. 1977.

26. Cox, C. S. and W. H. Munk, "Measurement of the roughness of the sea surface from photographs of the sun glitter," *J. Opt. Soc. Am.*, Vol. 44, No. 11, 838–850, 1954.
27. Aragón, S. R. and M. Elwenspoek, "Mie scattering from thin spherical bubbles," *J. Chem. Phys.*, Vol. 77, No. 7, 3406–3413, Oct. 1982.